

# The AGN nature of 11 out of 12 *Swift*/*RXTE* unidentified sources through optical and X-ray spectroscopy

R. Landi<sup>1</sup>, N. Masetti<sup>1</sup>, L. Morelli<sup>2</sup>, E. Palazzi<sup>1</sup>, L. Bassani<sup>1</sup>, A. Malizia<sup>1</sup>, A. Bazzano<sup>3</sup>,  
A.J. Bird<sup>4</sup>, A.J. Dean<sup>4</sup>, G. Galaz<sup>2</sup>, D. Minniti<sup>2</sup>, and P. Ubertini<sup>4</sup>

## ABSTRACT

The *Swift* Burst Alert Telescope (BAT) is performing a high Galactic latitude survey in the 14–195 keV band at a flux limit of  $\sim 10^{-11}$  erg cm<sup>-2</sup> s<sup>-1</sup>, leading to the discovery of new high energy sources, most of which have not so far been properly classified. A similar work has also been performed with the *RXTE* slew survey leading to the discovery of 68 sources detected above 8 keV, many of which are still unclassified. Follow-up observations with the *Swift* X-ray Telescope (XRT) provide, for many of these objects, source localization with a positional accuracy of few arcsec, thus allowing the search for optical counterparts to be more efficient and reliable. We present the results of optical/X-ray follow-up studies of 11 *Swift* BAT detections and one AGN detected in the *RXTE* Slew Survey, aimed at identifying their longer-wavelength counterparts and at assessing their nature. These data allowed, for the first time, the optical classification of 8 objects and a distance determination for 3 of them. For another object, a more refined optical classification than that available in the literature is also provided. For the remaining sources, optical spectroscopy provides a characterization of the source near in time to the X-ray measurement. The sample consists of 6 Seyfert 2 galaxies, 5 Seyferts of intermediate type 1.2–1.8, and one object of Galactic nature - an Intermediate Polar (i.e., magnetic) Cataclysmic Variable. Out of the 11 AGNs, 8 ( $\sim 70\%$ ) including 2 Seyferts of type 1.2 and 1.5, are absorbed with  $N_{\text{H}} > 10^{22}$  cm<sup>-2</sup>. Up to 3 objects could be Compton thick (i.e.  $N_{\text{H}} > 1.5 \times 10^{24}$  cm<sup>-2</sup>), but only in one case (*Swift* J0609.1–8636) does all

---

<sup>1</sup>INAF – Istituto di Astrofisica Spaziale e Fisica Cosmica di Bologna, Via P. Gobetti 101, I-40129 Bologna, Italy

<sup>2</sup>Departamento de Astronomía y Astrofísica, Pontificia Universidad Católica de Chile, Casilla 306, Santiago 22, Chile

<sup>3</sup>INAF – Istituto di Astrofisica Spaziale e Fisica Cosmica di Roma, Via Fosso del Cavaliere 100, I-00330 Roma, Italy

<sup>4</sup>School of Physics and Astronomy, University of Southampton, Highfield, Southampton, SO17 1BJ, UK

the observational evidence strongly suggests this possibility. The present data demonstrate the capability of coordinated hard X-ray and optical observations to discover absorbed AGNs.

*Subject headings:* X-ray sources: general – Galaxies: Seyfert – Stars: cataclysmic variable — X-ray: individuals: Swift J0444.1+2813; Swift J0601.9–8336; Swift J0732.5–1331; Swift J0823.4–0457; Swift J0918.5+1618; Swift J1009.3–4250; Swift J1038.8–4942; Swift J1200.8+0650; Swift J1238.9–2720; Swift J1930.5+3414; Swift J1933.9+3258; XSS J12303–4232.

## 1. Introduction

Recently, significant progress has been made in surveying the extragalactic sky at photon energies above 10 keV. Observations at these energies are efficient for finding absorbed AGNs, as they probe heavily obscured regions/objects, i.e. those that could be missed in optical, UV and even soft X-ray surveys.

Quantifying the fraction of nearby absorbed AGNs, particularly those that have  $N_{\text{H}} > 1.5 \times 10^{24} \text{ cm}^{-2}$  (i.e. the ones in Compton thick regime), is necessary if one wants to understand the accretion history of the Universe and study a population of objects poorly explored so far. Furthermore, the distribution of column densities is a key parameter for estimating the contribution of AGNs to the X-ray cosmic diffuse background and for testing current unified theories. A number of surveys performed above  $\sim 10$  keV are now available and can be used to study absorption in AGNs.

The recent *RXTE* survey made in the 8–20 keV energy band using slew observations (Revnivtsev et al. 2004; Sazonov & Revnivtsev 2004) resulted in a list of 68 objects (above  $3\sigma$  level) down to a flux limit of about  $3.4 \times 10^{-11} \text{ erg cm}^{-2} \text{ s}^{-1}$ ; 14 of these detections are still unidentified and so lack optical classification, which is the first step in any survey work (but see Bikmaev et al. 2006). Furthermore, no information on the X-ray spectral shape of the less known objects is available.

An even greater step forward has been provided by the *Swift* BAT survey, which is sensitive in the 15–195 keV band above a flux of  $\sim 10^{-11} \text{ erg cm}^{-2} \text{ s}^{-1}$  (Markwardt et al. 2005). Although primarily devoted to the study of Gamma-Ray Bursts, *Swift* observes the sky in survey mode when it is not responding to these events; with a large field of view of  $> 2$  sr, galactic and extragalactic X-/ $\gamma$ -ray sources can thus be serendipitously detected. Preliminary results from the first three months of observations provided a first sample of 66 objects: 12 were Galactic sources and 45 extragalactic objects (44 AGNs and

the Coma cluster); the 9 remaining sources were not optically classified. After this initial work, a number of new detections have also been reported (Tueller et al. 2005; Kennea et al. 2005; Ajello et al. 2006a) and often the proposed counterpart is not optically classified or characterized in X-rays below 10 keV.

In parallel with our ongoing program of optical classification of *INTEGRAL* IBIS sources (Masetti et al. 2004, 2006a,b,c,d), we have included in our activities follow-up work on unclassified objects detected with *Swift* and *RXTE*. Here, we report on optical/X-ray follow-up observations of a sample of 11 *Swift* BAT detections (Tueller et al. 2005; Kennea et al. 2005; Ajello et al. 2006a,b; Grupe et al. 2006) plus of an AGN detected in the *RXTE* Slew Survey (Revnivtsev et al. 2006). Our optical spectroscopy allows for the first time the classification of 8 objects and a distance estimate for 3 of them; for another object a more refined optical classification than that available in the literature is also provided. Despite having already been classified in the literature, 3 more objects were re-observed in order to have information on their optical status closer in time to the X-ray measurements. Although for most, but not all, objects in the sample, X-ray spectroscopy was published in the form of Atels, we have repeated the analysis here in order to include more observations and to provide a more uniform data set. In some cases we find significant differences between the published results and our own analyses. In the case of Swift J0918.5+1618 we also retrieved and analyzed an archival *ASCA* observation in order to have more detailed information on the source X-ray spectrum and to solve the issues related to the possible Compton thick nature of this type 1 Seyfert (Ajello et al. 2006a).

The optical results presented in this paper and concerning the *Swift* sources supersede the preliminary and concise ones presented in the Atels by Masetti et al. (2006e) and Morelli et al. (2006).

## 2. X-ray observations and data analysis

In this Section we present X-ray observations acquired with the XRT (X-ray Telescope, 0.2–10 keV) on board the *Swift* satellite (Gehrels et al. 2004).

XRT data reduction was performed using the XRTDAS v. 1.8.0 standard data pipeline package (XRTPipeline v. 0.10.3), in order to produce screened event files. All data were extracted only in the Photon Counting (PC) mode (Hill et al. 2004), adopting the standard grade filtering (0–12 for PC) according to the XRT nomenclature. The log of all X-ray observations is given in Table 1. For each measurement, we report the position of the XRT source associated with the high energy emitting object seen with *Swift* BAT or with

*RXTE* PCA, its uncertainty at a 90% confidence level, the XRT observation date, the relative exposure time, the energy band adopted in the source spectral fitting (which may vary depending on the statistical quality of each exposure), and the corresponding source count rate. Images have been extracted in the 0.3–10 keV energy band and searched for significant excesses associated with the *Swift* BAT or *RXTE* PCA sources. In all cases, a single bright X-ray source was detected inside the BAT positional uncertainty; for the *RXTE* source, the bright object detected with XRT coincides with the proposed *ROSAT* counterpart (Revnivtsev et al. 2006). The only exception, Swift J0601.9–8636, was 3'.6 away from the BAT detection (Kennea et al. 2006), i.e. just marginally consistent with the BAT position. This source has recently been detected also by *INTEGRAL* IBIS and localized with a 5'.2 uncertainty by this instrument (Bird et al. 2007); the intersection of *Swift* BAT and *INTEGRAL* IBIS error boxes clearly indicates that only LEDA 18394 (also ESO 005–G004, box in Figure 1) is the counterpart of this high energy emitting object. The other possible counterpart (smaller circle in Figure 1) can be excluded as optical spectroscopy acquired with the same setup at the 1.5m CTIO telescope on February 19, 2007, shows that it is a star, likely of spectral type A, without any peculiar spectral characteristics, i.e. it is unlikely to emit X-rays above 10 keV.

Events for spectral and temporal analysis were extracted within a circular region of radius 20'', centered on the source position, which encloses about 90% of the PSF at 1.5 keV (see Moretti et al. 2004). The background was taken from various source-free regions close to the X-ray source of interest, using both circular/annular regions with different radii in order to ensure an evenly sampled background. In all cases, the spectra were extracted from the corresponding event files using the XSELECT software and binned using GRPPHA in an appropriate way, so that the  $\chi^2$  statistic could be applied. We used the latest version (v.008) of the response matrices and create individual ancillary response files (ARF) using XRTMKARF. Spectral analyses have been performed using XSPEC version 12.2.1, while for temporal analyses we adopted the XRONOS package (version 5.21).

Each individual observation was inspected in order to assess the presence of short-term variability. In only three cases did we find significant short-term changes (Swift J0444.1+2813, Swift J0732.5–1331 and Swift J1200.8+0650 with a rms variability of 20–40%, 10–30% and  $\sim 20\%$ , respectively), but the low statistical quality of the data prevented any spectral analysis within segments of these observations.

For sources with more than one pointing <sup>1</sup>, we first analysed individual spectra to search

---

<sup>1</sup>In a few cases some observations have not been considered because their poor statistics did not allow us to perform a reliable spectral analysis.

for variability, and then combined the data to improve the statistics.

In just a few cases (Swift J0918.5+1618, Swift J1009.3–4250 and Swift J1038.8–4942), we found significant changes in flux, but not in spectral shape, between different observing periods. To allow for these flux variations, fits to the combined data were performed with the power law normalization free to vary.

Due to the limited spectral signal often available, we first employed a simple model of a power law absorbed by both a Galactic (Dickey & Lockman 1990) and an intrinsic column density (our baseline). If this baseline model was not sufficient to fit the data, we then introduced extra spectral components as required.

The results of the analysis of both single and combined observations are reported in Table 2 and Table 3 respectively, where we list: the Galactic absorption according to Dickey & Lockman (1990); the column density in excess to the Galactic value; the photon index; the 2–10 keV flux; the reduced  $\chi^2$  of the best-fit model and the column density measured by fixing the spectral photon index to a canonical value for an AGN ( $\Gamma = 1.8$ ). We also list in Table 3 the parameters relevant to any extra spectral features (e.g. soft excess component and iron line) required by the data in a few sources. In particular, we have added: an unabsorbed power law component having the same photon index of the primary continuum in 3 type 2 AGNs (Swift J0444.1+2813, Swift J1009.3–4250 and Swift J1930.5+3414); a thermal component in the only galactic source in the sample (Swift J0732.5–1331); and an iron line in two AGN (Swift J1238.9–2720 and XSS J12303–4232). The extra power law could be interpreted as scattered emission, which is a spectral component often found in type 2 Seyferts (Risaliti 2002). All quoted errors correspond to a 90% confidence level for a single parameter of interest ( $\Delta\chi^2 = 2.71$ ).

In one case (Swift J0918.5+1618), we also used archival *ASCA* GIS (Gas Imaging Spectrometers, Ohashi et al. 1996) data to better characterize the source spectrum. The relevant spectra and associated files were downloaded from the TARTARUS database<sup>2</sup> and analyzed with the same XSPEC version used for the XRT data. For this particular case, the best-fit results are presented in Table 4.

Figures 2 to 12 show, for those AGN in the sample with high signal-to-noise ratio, the results of this spectral analysis, which are discussed in more details in the subsections devoted to each individual object. The X-ray spectra of the only galactic source in the sample (Swift J0732.5–1331) are presented and discussed in the Appendix.

---

<sup>2</sup>available at  
<http://tartarus.gsfc.nasa.gov/>

### 3. Optical observations and data analysis

Sources with  $\text{Dec} > -20^\circ$  were observed spectroscopically at the Bologna Astronomical Observatory in Loiano (Italy) with the 1.5-metre telescope “G.D. Cassini” equipped with the BFOSC instrument, which uses a  $1300 \times 1340$  pixel EEV CCD. In all observations, Grism #4 and a slit width of  $2''$  were used, providing a  $3500\text{--}8700 \text{ \AA}$  nominal spectral coverage. The use of this setup secured a final dispersion of  $4.0 \text{ \AA/pix}$  for all these spectra. Spectroscopic observations of the remaining southern sources were secured with the 1.5-metre CTIO telescope of Cerro Tololo (Chile) equipped with the R-C spectrograph, which carries a  $1274 \times 280$  pixel Loral CCD. Data were acquired using Grating #13/I and with a slit width of  $1''.5$ , giving a nominal spectral coverage between  $3300$  and  $10500 \text{ \AA}$  and a dispersion of  $5.7 \text{ \AA/pix}$ . In one case (Swift J1009.3–4250 = ESO 263–13) we retrieved an archival optical spectrum, with dispersion  $1.6 \text{ \AA/pix}$ , acquired with the 4-metre Anglo-Australian Telescope (AAT) within the 6dF Galaxy Survey (Jones et al. 2004); we refer the reader to this latter paper for observational details. The complete log of the observations is reported in Table 5.

After cosmic-ray rejection, the Loiano and CTIO spectra were reduced, background subtracted and optimally extracted (Horne 1986) using IRAF<sup>3</sup>. Wavelength calibration was performed using He-Ar lamps acquired soon after each spectroscopic exposure; the Loiano spectra were then flux-calibrated using the spectrophotometric standard BD+25°3941 (Stone 1977), whereas the CTIO spectra used the standard star LTT 7379 (Hamuy et al. 1992, 1994). Finally, and when applicable, different spectra of the same object were stacked together to increase the S/N ratio. The wavelength calibration uncertainty was  $\sim 0.5 \text{ \AA}$  for all cases; this was checked using the positions of background night sky lines. Instrumental broadening of spectral features is (in terms of  $\sigma$  assuming a Gaussian description)  $\approx 260 \text{ km s}^{-1}$  and  $\approx 300 \text{ km s}^{-1}$  for the Loiano and CTIO spectra, respectively.

To flux calibrate the optical spectrum of Swift J1009.3–4250 (originally expressed in counts) we considered the  $B$  and  $R$  magnitudes of Winkler & Payne (1990), which were acquired on a  $30''$  circular region centered on the source, and rescaled them to the 6dF optical fibre aperture ( $6''.7$  in diameter). This was done using the SuperCosmos (Hambly et al. 2001) digitized images and the conversions from the SuperCosmos to the Johnson-Cousins photometry system (Colless 2003). We then used these rescaled magnitudes to convert the spectrum counts into physical units. For the AGN classification, we used the criteria of Veilleux & Osterbrock (1987) and the line ratio diagnostics of Ho et al. (1993,

---

<sup>3</sup>IRAF is the Image Reduction and Analysis Facility made available to the astronomical community by the National Optical Astronomy Observatories, which are operated by AURA, Inc., under contract with the U.S. National Science Foundation. It is available at <http://iraf.noao.edu/>

1997); moreover, for the subclass assignation of Seyfert 1 nuclei, we used the  $H_\beta/[O\text{ III}]\lambda 5007$  line flux ratio criterion as in Winkler (1992).

The quoted optical magnitudes are extracted from the USNO-A2.0<sup>4</sup> catalog. Table 6 reports the emission line fluxes of the most interesting lines in each spectrum. The line fluxes and absolute magnitudes from extragalactic sources presented in this paper were dereddened for Galactic absorption along their line of sight following the prescription for the computation of the Galactic color excess  $E(B - V)_{\text{Gal}}$  (also reported in Table 6) as in Schlegel et al. (1998) and assuming the Galactic extinction law of Cardelli et al. (1989). For the intrinsic reddening calculations, we assumed an intrinsic  $H_\alpha/H_\beta$  line ratio of 2.86 (Osterbrock 1989). The spectra of the galaxies shown here were not corrected for starlight contamination (see, e.g., Ho et al. 1993, 1997) given their limited S/N and resolution. We do not consider this to affect any of our conclusions. We have also compared, in Table 6, the extinction obtained from the optical ( $A_{V_{\text{opt}}}$ ) and X-ray data ( $A_{V_X}$ ). When this is possible, we find that  $A_{V_{\text{opt}}}$  is generally smaller than  $A_{V_X}$ ; for AGN this is not a new result as it was first noticed by Maccacaro et al. (1982). The cause of this discrepancy is not clear, but could be due to the optical and X-ray absorption coming from different media/regions (Weingartner & Murray 2002) or due to a dust to gas ratio or dust grain dimensions different than in our galaxy (Maiolino et al. 2001). Only in one case (Swift J0601.9–8636) do we find that  $A_{V_X}$  is smaller than  $A_{V_{\text{opt}}}$ , but this may be due a false estimate of the absorption column density in the X-ray spectrum (see Section 5.2) and the likely Compton thick nature of this source (see Section 5.2).

Figures 13 and 14 show the optical spectra of all AGN in the sample, while the optical spectrum of the galactic source Swift J0732.5–1331 is presented in the Appendix.

#### 4. Diagnostic ratios

To further characterize our objects, we have used diagnostic diagrams to confirm the presence of an active nucleus and to discriminate between Compton thin and thick sources. It is in fact possible in some cases that the AGN component is so deeply absorbed that other components, such as a starburst, dominate in the optical spectrum (Masetti et al. 2006c). Since the IR emission is generally associated with star-forming activity while the  $[O\text{ III}]$  emission is mainly produced by photons generated in the active nucleus, we can employ the  $L_{[O\text{ III}]} / L_{\text{IR}}$  ratio to discriminate between AGN and Starburst galaxies. Indeed, in the Ho

---

<sup>4</sup>available at  
<http://archive.eso.org/skycat/servers/usnoa/>

et al. (1997) sample of nearby galaxies, 90% of those classified as starbursts have a value of  $L_{[\text{O III}]} / L_{\text{IR}}$  below  $10^{-4}$ , while 88% of the AGN have ratios above this value (Panessa and Bassani 2002).

Generally, indirect arguments are used to probe the Compton thick versus thin nature of a type 2 AGN, and these include the equivalent width of the iron line, and the ratio of anisotropic (i.e. modified by absorption such as the 2–10 keV emission) versus isotropic (i.e. not modified by absorption) luminosities. The  $[\text{O III}]\lambda 5007$  ( $[\text{O III}]$  hereafter) flux is considered as a good isotropic indicator because it is produced in the Narrow Line Regions, which are not strongly affected by absorption (Maiolino & Rieke 1995; Risaliti et al. 1999; Bassani et al. 1999). The  $L_X / L_{[\text{O III}]}$  ratio has been studied in a large sample of Seyfert 2 galaxies; all Compton thin Seyfert (type 1 and 2) show ratios higher than 1, while Compton thick sources show  $L_X / L_{[\text{O III}]}$  ratios below this value (Bassani et al. 1999).

Another isotropic indicator is the Far-Infrared (FIR) emission which is probably produced in even more external regions; typically, type 1 and Compton thin type 2 AGNs show  $L_X / L_{\text{IR}}$  ratios around or above 0.1, while Compton thick type 2 objects show ratios lower than  $5 \times 10^{-4}$  (David et al. 1992; Mulchaey et al. 1994; Risaliti et al. 1999). However, the validity of this diagnostic is less certain because many components besides the nuclear one (for example coming from star-burst activity and from the host galaxy) may contribute to the IR flux. These caveats should be kept in mind when dealing with this particular ratio.

Finally, emission above 20 keV can be used as an isotropic probe too as it is virtually unaffected by absorption as long as  $\log N_{\text{H}}$  is below 24.5; for higher column density even the emission above 20 keV is blocked and can only be seen indirectly. Using a sample of hard X-ray selected AGN, Malizia et al. (2007) found that the  $L_X / L_{\text{HX}}$  ratio of type 1 AGN is typically around 0.7, decreasing progressively as the absorption increases; Compton thick objects are easily recognized for having negligible absorption and a ratio below 0.02.

In conclusion, these four ratios can provide an independent way to establish which is the dominant component between AGN and Starburst and, at the same time, they are a powerful tool in the detection of Compton thick sources when the X-ray spectral analysis is not sufficient to recognize them. Here, the optical spectra provide information on the  $[\text{O III}]$  flux and the X-ray spectroscopy on the X-ray one. Hard X-ray fluxes in the 10–100 keV energy band are instead obtained from available *Swift* BAT observations (see references in Table 7). When possible, the  $[\text{O III}]$  flux of each galaxy has been corrected for extinction assuming the absorption local to the narrow-line region as determined from the  $\text{H}_\alpha / \text{H}_\beta$  line



ratio<sup>5</sup> (Bassani et al. 1999); the X-ray and hard X-ray fluxes are instead not corrected for absorption. IR fluxes have been estimated from *IRAS* data extracted from the NASA/IPAC Extragalactic Database<sup>6</sup> (NED) archive or from the HEASARC archive. For this paper, we adopt the same definition used in Mulchaey et al. (1994) to estimate the IR flux:  $F(\text{IR}) = S_{25\ \mu\text{m}} \times (\nu_{25\ \mu\text{m}}) + S_{60\ \mu\text{m}} \times (\nu_{60\ \mu\text{m}})$ . The IR fluxes together with the hard X-ray fluxes estimated in this way, as well as the luminosity ratios used in the present study are all listed in Table 7.

Using these ratios, we can conclude that most AGN in the sample are dominated by an active nucleus rather than by starburst activity. Furthermore, they are mostly characterized by being in the Compton thin regime. Three objects could be Compton thick, but only in one case (Swift J0601.9+8336) does all the observational evidence strongly suggest this possibility.

## 5. Results on individual sources

In the following subsections, we present X-ray and optical results of all AGN analyzed in this paper. The only galactic source found is discussed separately in the Appendix. We have assumed a cosmology with  $H_0 = 65\ \text{km s}^{-1}\ \text{Mpc}^{-1}$ ,  $\Omega_\Lambda = 0.7$  and  $\Omega_m = 0.3$ .

### 5.1. Swift J0444.1+2813

This BAT source is identified with the 2MASS (Two Micron All Sky Survey, Skrutskie et al. 2006) extended object 2MASX J04440903+2813003 (Tueller et al. 2005), associated with an unclassified principal galaxy (PGC 86269 at  $z = 0.011268$ ; Pantoja et al. 1997). It is listed in the NVSS (National Radio Astronomy Observatory [NRAO] Very Large Array [VLA] Sky Survey Catalog; Condon et al. 1998) with a 20 cm flux of  $28.6 \pm 0.9\ \text{mJy}$ . The object is also an *IRAS* source and has never been detected at X-ray energies before. A preliminary analysis of the XRT data indicated heavy absorption ( $N_H \sim 10^{23}\ \text{cm}^{-2}$ ), but did not provide any information on the source spectral shape (Tueller et al. 2005). The XRT spectra are all well fitted with two power laws having the same photon index but with only one intrinsically absorbed (see Table 3 and Figure 2). The addition of an unabsorbed

---

<sup>5</sup> $F_{[\text{OIII}],\text{corr}} = F_{[\text{OIII}],\text{obs}} \left[ \frac{\left(\frac{H_\alpha}{H_\beta}\right)}{\left(\frac{H_\alpha}{H_\beta}\right)_0} \right]^{2.94}$ , where  $\left(\frac{H_\alpha}{H_\beta}\right)_0 = 3$

<sup>6</sup>available at <http://nedwww.ipac.caltech.edu/>

power law component takes into account excess emission below 2 keV and is required by the data with a significance greater than the 99.73% confidence level in each observation ( $> 99.99\%$  for the combined spectrum). The primary power law is flat and absorbed by an intrinsic column density of  $\sim 4 \times 10^{22} \text{ cm}^{-2}$ . The absorption is lower than the preliminary value reported by Tueller et al. (2005).

Optical spectroscopy of the object shows the presence of narrow  $\text{H}_\alpha$ ,  $[\text{N II}]$ ,  $[\text{S II}]$ ,  $[\text{O I}]$  and  $[\text{O III}]$  emission lines, with Full Width at Half Maximum (FWHM)  $\lesssim 800 \text{ km s}^{-1}$  (Figure 13, upper left panel), superimposed on a reddened continuum. All features are at redshift  $z = 0.011 \pm 0.001$ , consistent with the 21 cm radio measurement of Pantoja et al. (1997). This corresponds to a luminosity distance  $D_L = 51.2 \text{ Mpc}$  and gives a luminosity of  $(3.1\text{--}3.8) \times 10^{42} \text{ erg s}^{-1}$  in the 2–10 keV energy band. The narrowness of the lines and their relative strengths indicate that this is a Seyfert 2 galaxy. The  $3\sigma$  upper limit on the Balmer decrement ( $> 74$ ) implies a dereddened  $[\text{O III}]$  flux  $F_{[\text{OIII}]} > 1.4 \times 10^{-9} \text{ erg cm}^{-2} \text{ s}^{-1}$ . The latter measurement, if compared with the X-ray flux, implies that this source is in the Compton thick regime (see Table 7); however, the  $L_X/L_{\text{IR}}$  and  $L_X/L_{\text{HX}}$  ratios are typical of Compton thin sources and the upper limit ( $EW < 110 \text{ eV}$ ) on the 6.4 keV iron line, which can be obtained from the X-ray data, excludes a Compton thick object; also the short-term variability seen in the XRT data argues against a Compton thick nature.

## 5.2. Swift J0601.9–8636

Despite being a principal galaxy, the optical counterpart of this *Swift* AGN (LEDA 18394 also ESO 005–G004), is still unclassified in the optical. The source is a radio emitter, being reported in the SUMSS (Sidney University Molonglo Sky Survey; Mauch et al. 2003) catalog with a 36 cm flux of  $119.3 \pm 4.5 \text{ mJy}$  and as a Parkes source with a 4850 MHz flux of  $30 \pm 5 \text{ mJy}$ ; it is fairly bright and extended in the infrared, being listed both in the *IRAS* bright galaxy sample (Sanders et al. 2003) and in the extended 2MASS catalog. Up to now, no X-ray data have been reported from this object.

If we fit the XRT spectrum with an absorbed power law with  $\Gamma = 1.8$ , we do not find any evidence for extra absorption in excess of the Galactic value (see Table 2).

From the nucleus of this galaxy, we detect narrow (FWHM  $\lesssim 650 \text{ km s}^{-1}$ ) emission lines of  $\text{H}_\alpha$ ,  $[\text{N II}]$  and  $[\text{S II}]$  superimposed on a continuum resembling that typical of a spiral galaxy (Figure 13, upper right panel). The  $\text{H}_\alpha/[\text{N II}]$  flux ratio is consistent with that typical of Seyfert 2 galaxies, although this observable alone cannot be used to discriminate the nature of this source. However, the radio emission and the detection above 20 keV

strongly suggest that we are dealing with an active galaxy. We are therefore led to conclude that Swift J0601.9–8636 is probably a hidden Seyfert 2 galaxy. The estimated redshift is  $z = 0.006 \pm 0.001$ , consistent with that measured by Fisher et al. (1995). This redshift corresponds to a luminosity distance  $D_L = 29.7$  Mpc, implying  $L_{(2-10 \text{ keV})} = 1.2 \times 10^{40} \text{ erg s}^{-1}$ . This luminosity is unusually low compared to that above 20 keV ( $3.9 \times 10^{42} \text{ erg s}^{-1}$ ), suggesting again extreme absorption.

The non-detection of  $H_\beta$  implies a  $H_\alpha/H_\beta$  flux ratio  $3\sigma$  upper limit of 38.3, which in turn means  $A_V > 8.1$  and a hydrogen column  $N_H > 1.5 \times 10^{22} \text{ cm}^{-2}$  local to the galaxy nucleus, which is somewhat at odds with the result of the (admittedly with low S/N) X-ray data, unless the source is in the Compton thick regime.

The non-detection of [O III], together with the lower limit on the reddening local to the source makes the [O III] flux value (or a limit thereof) unconstrained, and so are the  $L_{\text{IR}}/L_{[\text{OIII}]}$  and  $L_X/L_{[\text{OIII}]}$  ratios. The observed  $L_X/L_{\text{IR}}$  and  $L_X/L_{\text{HX}}$  ratios are instead well constrained and their very small values are compatible with Swift J0601.9–8636 being a Compton thick AGN; although the small  $L_X/L_{\text{IR}}$  value is also consistent with a starburst-powered galaxy, the optical spectrum provides a  $H_\alpha/[\text{N II}]$  ratio compatible with those of type 2 Seyfert galaxy. Indeed, a recent *Suzaku* observation of this source has confirmed its Compton thick nature (Ueda et al. 2007).

### 5.3. Swift J0823.4–0457

The XRT position of this BAT source (Ajello et al. 2006a) falls exactly on the galaxy Fairall 272 (also PGC 023515 and MCG–01–22–006), which belongs to a peculiar interacting system and is part of a medium-poor cluster of galaxies in the constellation Hydra (Fairall 1979). This galaxy (still optically unclassified) shows strong [O III]  $\lambda\lambda 4959, 5007$  as well as narrow  $H_\beta$  emission lines, produced in a region wider than the galaxy core (maybe chaotic filaments). These emission lines, combined with the spectral features observed in the two other neighboring interacting galaxies (Fairall 271 and Fairall 273), suggest that Fairall 272 hosts an active nucleus of unknown class (the filaments could be associated with ejective or explosive processes).

Fairall 272 is also a radio emitter, detected in the NVSS catalog with a 20 cm flux of  $37.2 \pm 1.5 \text{ mJy}$ ; as none of the other nearby galaxies is detected at this frequency, it is likely that Fairall 272 is the most active galaxy of the group. An *IRAS* source (IRAS 08205–0446), located only  $0'.6$  away, is likely associated with Fairall 272.

A preliminary analysis of the XRT data indicate that the X-ray spectrum is either flat

with negligible absorption, or a more canonical one ( $\Gamma = 2$ ), but absorbed ( $N_{\text{H}} \sim 10^{23} \text{ cm}^{-2}$ ; Ajello et al. 2006a). The results of our spectral analysis confirm these previous findings: a flat ( $\Gamma \sim 0.7$ ) unabsorbed power law is a good description of the XRT data ( $\Delta\chi^2/\nu = 7.8/13$ , but since we cannot put any constraint on the photon index, we prefer to fix  $\Gamma = 1.8$  in the fitting procedure and estimate the absorption local to the source (see Table 2).

The optical spectrum of Fairall 272 shows narrow ( $\text{FWHM} \lesssim 750 \text{ km s}^{-1}$ )  $\text{H}_\alpha$ ,  $\text{H}_\beta$ ,  $[\text{N II}]$ ,  $[\text{S II}]$ ,  $[\text{OI}]$  and  $[\text{O III}]$  emission lines over a flat continuum (Figure 13, central left panel). These features put the source at redshift  $z = 0.023 \pm 0.001$ , consistent with the measurement of Fouque et al. (1992), which implies a luminosity distance  $D_L = 108 \text{ Mpc}$  and a 2–10 keV luminosity of  $5.9 \times 10^{42} \text{ erg s}^{-1}$ . In this case also, the line shapes and ratios indicate that this is a Seyfert 2 galaxy. In view of the optical classification an absorbed power law is preferred to an unabsorbed flat spectrum.

The  $\text{H}_\alpha/\text{H}_\beta$  flux ratio of 6.1 provides a dereddened  $[\text{O III}]$  flux of  $2.4 \times 10^{-13} \text{ erg cm}^{-2} \text{ s}^{-1}$  and the diagnostic ratios indicate that this is a Compton thin AGN (see Table 7). This substantially confirms the X-ray characterization of the source as a not heavily absorbed AGN.

#### 5.4. Swift J0918.5+1618

This *Swift* object coincides with the galaxy Mrk 704 ( $z = 0.029$ ; e.g., Hewitt & Burbidge 1991), which has been detected earlier in X-rays by *ROSAT* (Schwope et al. 2000) and *ASCA*, and is listed in the *RXTE* Slew Survey (Revnivtsev et al. 2004). This galaxy is detected in the radio by the NVSS survey with a 20 cm flux of  $6.1 \pm 0.5 \text{ mJy}$ ; it is also an IRAS source and a 2MASS extended object.

The source has been classified in the literature as a Seyfert galaxy but of different types ranging from 1 to 1.5 (see for example a compendium in Nagao, Taniguchi & Murayama 2000); it is also considered a peculiar type of Seyfert 1 AGN (i.e. a “polar scattered” object) as it has spectropolarimetric properties consistent with those found in type 2 Seyfert galaxies despite its type 1 optical classification (Nagao, Taniguchi & Murayama 2000). According to recent modeling, “polar scattered” Seyfert 1 are those viewed at an inclination very close to  $45^\circ$ , such that the line of sight passes through the outer layers of the torus whereas type 1 and 2 Seyfert galaxies have inclinations lower and greater than  $45^\circ$  respectively (Smith et al. 2004; Hoffman et al. 2005).

This latter fact seems to be more consistent with an intermediate optical classification: given that the Broad Line Region (BLR) is obscured by a dusty torus, the emission lines

would appear with a composite profile consisting of both narrow and broad emissions.

The X-ray information on this object also suggests that we are dealing with a peculiar object. Ajello et al. (2006a) reported inconsistencies between the BAT and XRT spectra and further suggested, through the analysis of archival *ASCA* data, that the source might be in the Compton thick regime, in contrast with its optical classification as a type 1 AGN.

This prompted our optical follow-up observations in order to assess the spectral characteristics of this object relatively close in time to the *Swift* measurement.

Due to the low statistical quality of the first XRT observation, only the last three measurements have been taken into account for the spectral analysis. All data sets are compatible with each other being well fitted with a steep ( $\Gamma \sim 1.8\text{--}1.9$ ) power law having mild absorption (see Table 2). There was a change in flux ( $\sim 60\%$ ) between the three XRT observations separated by a few months, but no variation within the individual measurements.

Broad He I, He II, Fe I, and Balmer emissions at least up to  $H_\zeta$  ( $\text{FWHM}_{H_\beta} \sim 5500 \text{ km s}^{-1}$ ), as well as narrow  $H_\alpha$ ,  $H_\beta$ , [N II], [S II], [O I], [O III] and [Ne III] emission lines are detected in the optical spectrum of Swift J0918.5+1618 (Figure 13, central right panel), which moreover shows a blue continuum. The spectrum, and a  $H_\beta$ /[O III] flux ratio of ( $\sim 2.3$ ), together imply a Seyfert 1.2 AGN classification for this galaxy. From the observed wavelengths of narrow features, we determine a redshift  $z = 0.028 \pm 0.001$ , in agreement with previous measurements. This gives a luminosity distance  $D_L = 131.9 \text{ Mpc}$  to the source. At a redshift  $z = 0.028$ , the 2–10 keV luminosity of Swift J0918.5+1618 was  $1.6 \times 10^{43} \text{ erg s}^{-1}$  at the time of the XRT observation.

Clearly, our optical and X-ray results are at odds with the conclusions of Ajello et al. (2006a), suggesting the use of *ASCA* data to get a more detailed picture of the source X-ray spectrum.

*ASCA* observed Swift J0918.5+1618 on May 12 1998 for an effective exposure time, for the GIS instrument, of  $\sim 38 \text{ ks}$ . A fit to the GIS spectra with a simple power law seen through Galactic absorption provides a poor fit to the data ( $\chi^2/\text{d.o.f.} = 247.7/194$ ) and a flat photon index ( $\Gamma \sim 1$ ), suggesting the presence of more complex absorption. We therefore applied a partial covering model, as observed in other intermediate Seyfert galaxies like Mrk 6 (Malizia et al. 2003), Mrk 1152 (Quadrelli et al. 2003) and 4U 1344–60 (Piconcelli et al. 2006).

The addition of this component strongly improves the  $\chi^2$  value, being significant at more than 99.99% confidence level ( $\Delta\chi^2 = 43.2$  for two degrees of freedom). Inspection of the residuals around the expected iron line position suggests the presence of such a feature.

In fact, the inclusion of this extra component further improves the fit ( $\Delta\chi^2 = 11.0$  for two degrees of freedom) and gives a column density of  $\sim 13 \times 10^{22} \text{ cm}^{-2}$  covering  $\sim 61\%$  of the source (see in Figure 3 and a narrow line at 6.4 keV with an  $EW$  of  $\sim 233 \text{ eV}$ , which is typical of Seyfert 1 galaxies (Turner et al. 1997). With this best-fit model (see Table 4 and Figure 4), the power law photon index is 1.5, similar to that observed in other AGN showing complex absorption. Extrapolation of the *ASCA* best-fit to the 10–100 keV energy band provides a flux consistent with the BAT one.

In order to search for consistency between the *ASCA* and XRT results, we re-fitted the whole XRT data set with the *ASCA* best-fit model, finding an equally acceptable fit ( $\chi^2/\nu = 89.0/91$ ); however, in this case, the column density was much lower ( $\sim 10^{22} \text{ cm}^{-2}$ ) while the covering fraction was compatible with the *ASCA* measurement. This is very similar to what has been observed in similar sources where the absorption changes but the covering fraction remains constant (see, for example, Malizia et al. 2003 for Mrk 6). It also explains why the 2–10 keV flux observed by *Swift* XRT, *ASCA* and *RXTE* (Revnivtsev et al. 2004) is highly variable, by about a factor of 2 on long ( $\sim$ years) time-scales, with the XRT measurement being in the middle of the range of the observed values,  $(\sim 0.5\text{--}1.4) \times 10^{-11} \text{ erg cm}^{-2} \text{ s}^{-1}$ .

To conclude, it is important to stress that this source is not Compton thick, but more likely an absorbed intermediate Seyfert 1 galaxy, where the BLR is observed through the upper layers of the torus. This is further confirmed by our diagnostic ratios, which locate the object in a region populated by Compton thin Seyfert galaxies (see Table 7).

### 5.5. Swift J1009.3–4250

This *Swift* source (Ajello et al. 2006b) coincides in position with ESO 263–13 (= Fairall 427), a face-on spiral galaxy at redshift  $z=0.0333\pm0.0003$ , classified as a Seyfert 2 galaxy (Fairall 1983); it is a peculiar source as it has a double nucleus (Gimeno et al. 2004) and it shows an extended ionized nebulosity (Durret 1989). This object is also a radio emitter, detected in the SUMSS catalog with a 36 cm flux of  $23.1 \pm 1.1 \text{ mJy}$ , and it is listed in the extended 2MASS catalog.

According to Ajello et al. (2006b), a model including an absorbed power law plus a reflection component (PEXRAV model in XSPEC) provides a good description of the combined XRT/BAT spectra, yielding a photon index  $\Gamma \sim 2$  and a lower limit for the absorbing column density of  $\sim 10^{24} \text{ cm}^{-2}$ , again suggesting a Compton thick nature.

Our XRT data of Swift J1009.3–4250 are well described by our baseline model plus

another power law, having the same photon index, but absorbed only by the Galactic column density; the extra power law component is required (at a confidence level  $> 99.99\%$  in the combined spectrum and in the range  $95.4\text{--}99.99\%$  in each single pointing) to account for excess emission observed below 2 keV (see Figure 5). The observed column density is  $3\text{--}4 \times 10^{23} \text{ cm}^{-2}$ , well below the Compton thick regime. We also found a flux variation of  $\sim 50\%$  among the XRT observations, but no evidence for spectral changes.

The 6dF optical spectrum of ESO 263–13 shows a flat continuum with the presence of narrow Balmer, He II, [N II], [S II], [O I], [O II] and [O III] emissions, with FWHM  $\lesssim 600 \text{ km s}^{-1}$  (Figure 13, lower left panel) and at a redshift  $z = 0.0335 \pm 0.0001$  (Jones et al. 2004), which is consistent with the result of Fairall (1983). This corresponds to a luminosity distance  $D_L = 159 \text{ Mpc}$  and gives a luminosity of  $(4.5\text{--}8.4) \times 10^{42} \text{ erg s}^{-1}$  in the 2–10 keV energy band. The narrowness of the lines and their relative strengths as seen in the 6dF spectrum confirm the Seyfert 2 nature of this galaxy.

The  $H_\alpha/H_\beta$  flux ratio of 4.0 provides an optically dereddened [O III] flux of  $F_{[\text{O III}]} = 2.7 \times 10^{-13} \text{ erg cm}^{-2} \text{ s}^{-1}$  which, when compared with the 2–10 keV X-ray flux, implies an AGN in the Compton thin regime (see Table 7). This is confirmed by the  $L_X/L_{\text{HX}}$  ratio, which, although low, is nevertheless compatible with the observed column density. We therefore rule out the Compton thick hypothesis put forward by Ajello et al. (2006b).

## 5.6. Swift J1038.8–4942

This source (Tueller et al. 2005) is likely associated with an extended 2MASS object (2MASX J10384520–4946531), which is identified with an unclassified galaxy. No redshift is known, and no radio emission has so far been reported from this object. The source is also listed in the *ROSAT* All Sky Survey Bright Source Catalog (Voges et al. 1999) and is associated with an *IRAS* object.

Preliminary analysis of the XRT data (Tueller et al. 2005) provided information only on the absorption ( $N_{\text{H}} \sim 10^{22} \text{ cm}^{-2}$ ). Our analysis indicates either a flat spectrum and lower absorption or a more canonical one with a similar column density (see Table 2 and Figure 6); furthermore, we detect variations in flux of  $\sim 10\text{--}30\%$  between observations.

Optical spectroscopy of this object shows broad  $H_\alpha$  and  $H_\beta$  emissions (FWHM $_{H_\beta} \sim 6700 \text{ km s}^{-1}$ ) with a narrow component on top; moreover, narrow [N II], [S II], [Ne III], [O I] [O II] and [O III] emission lines are detected on a relatively flat continuum (Figure 13, lower right panel). The  $H_\beta/[O \text{ III}]$  flux ratio, 1.7, allows us to classify this galaxy as a Seyfert of type 1.5. From the observed wavelengths of narrow features, we determine for the first

time a redshift  $z = 0.060 \pm 0.001$  for this galaxy, which means a luminosity distance  $D_L = 289.3$  Mpc. This corresponds to a 2–10 keV luminosity range  $(7.8\text{--}11.7) \times 10^{43}$  erg s $^{-1}$  and, assuming a magnitude  $B \sim 16.1$  and no local absorption in the optical, an absolute  $B$ -band magnitude  $M_B \sim -23.2$ .

Given its optical classification, this object is obviously Compton thin, as confirmed by our diagnostic ratios; it is, however, another interesting case of an intermediate Seyfert with intrinsic absorption.

### 5.7. Swift J1200.8+0650

This BAT source (Kennea et al. 2005) has been associated with PGC 037894 (also CGCG 041–020 and LEDA 37894), a principal galaxy at redshift  $z = 0.036$ , which has not been optically classified yet. The source is a weak radio emitter detected in the NVSS and FIRST (Faint Images of the Radio Sky at Twenty-centimeters, White et al. 1997) surveys with a 20 cm flux in the range 5–6 mJy; like other AGNs of our sample, it is an *IRAS* faint source and a 2MASS extended object.

In this case, no X-ray emission has so far been reported. Individual or combined X-ray data provide an acceptable fit with an absorbed power law having a column density of  $(6\text{--}8) \times 10^{22}$  cm $^{-2}$  and a photon index in the range 1.3–1.8 (see Table 2 and Figure 7).

The addition of a narrow Gaussian Fe K $\alpha$  line in the XRT spectrum of the first observation (thicker crosses in Figure 7) does not significantly improve the quality of the fit ( $\Delta\chi^2 = 7.1$  for 2 degrees of freedom or  $> 95.4\%$  confidence level), but returns a line energy of  $E \sim 6.3$  keV and an  $EW$  of  $\sim 266$  eV, much in line with other AGN measurements of this feature. It is likely that a longer dedicated exposure could provide further insight on the presence of this feature.

The optical spectrum of PGC 037894 shows H $\alpha$ , H $\beta$ , [N II], [S II] and [O III] narrow (FWHM  $\lesssim 850$  km s $^{-1}$ ) emission lines over a flat continuum (Figure 14, upper left panel). The features are at redshift  $z = 0.035 \pm 0.001$ , consistent with Grogin, Geller & Huchra (1998), which corresponds to a luminosity distance  $D_L = 165.8$  Mpc and gives a  $1.9 \times 10^{43}$  erg s $^{-1}$  2–10 keV luminosity for this source. Again, the line shapes and ratios indicate that this is a Seyfert 2 galaxy.

The H $\alpha$ /H $\beta$  flux ratio  $3\sigma$  upper limit ( $> 4.7$ ) implies a dereddened [O III] flux  $F_{[\text{OIII}]} > 2.9 \times 10^{-14}$  erg cm $^{-2}$  s $^{-1}$ . The diagnostic ratios, and also the possible iron line  $EW$  value, place this source well in the Compton thin regime, indicating that is a classical type 2 AGN.



### 5.8. Swift J1238.9–2720

This source (Tueller et al. 2005) is associated with the optically unclassified galaxy ESO 506–G027, at  $z = 0.025$  (Da Costa et al. 1998). This is a radio emitter with a 20 cm flux of  $73.7 \pm 2.3$  mJy in the NVSS survey. This galaxy is also an *IRAS* faint source and it is an extended 2MASS object.

A preliminary analysis of the XRT data indicated that it might be a Compton thick object showing strong absorption ( $N_{\text{H}} \sim 10^{23} \text{ cm}^{-2}$ ) and an iron line with  $EW$  of about 500 eV (Tueller et al. 2005). The data indicate a change in flux ( $\sim 20\%$ ) between the first and second observations on a time-scale of a few months (see Table 3); this evidence casts some doubts on the Compton thick nature of the source as the reflection component, if due to the torus, is expected to provide flux changes on longer time-scales. Individual and combined spectra are not of sufficient quality to allow a constraint on the photon index which was therefore fixed to the canonical value of 1.8; the observed column density is  $\sim 10^{23} \text{ cm}^{-2}$  and a narrow iron line is detected with  $> 99.73\%$  confidence ( $\Delta\chi^2 = 21.1$  for 5 degrees of freedom) (see Figure 8). The two-dimensional iso- $\chi^2$  contour plot of line intensity versus energy is shown in Figure 9. The line has an  $EW$  of 500 eV which does not necessarily imply that we are dealing with a Compton thick AGN, as a similar value is also compatible with the observed column density (Turner et al. 1997).

The optical spectrum (Figure 14, upper right panel) of this source may help in assessing its Compton nature. The presence of  $\text{H}_\alpha$ ,  $\text{H}_\beta$ ,  $[\text{N II}]$  and  $[\text{O III}]$  narrow (FWHM  $\lesssim 1000 \text{ km s}^{-1}$ ) emission lines detected on a spiral galaxy continuum and the overall spectral appearance indicate that this source is most likely a Seyfert 2 galaxy. All emission features are at redshift  $z = 0.024 \pm 0.001$ , consistent with Da Costa et al. (1998). This implies a luminosity distance  $D_L = 112.7 \text{ Mpc}$  and a  $(6.4\text{--}8.2) \times 10^{42} \text{ erg s}^{-1}$  2–10 keV luminosity range for this galaxy.

The  $\text{H}_\alpha/\text{H}_\beta$  flux ratio  $3\sigma$  upper limit of  $> 23$ , gives a dereddened  $[\text{O III}]$  flux greater than  $1.2 \times 10^{-11} \text{ erg}$ .

The flux ratios provide contradictory results as the  $L_{\text{X}}/L_{[\text{O III}]}$  indicates a Compton thick nature, while the  $L_{\text{X}}/L_{\text{IR}}$  and  $L_{\text{X}}/L_{\text{HX}}$  provide evidence for a thin behavior. However, the observed column density is sufficient to explain the low values of the first ratio: very likely, this is a borderline object in between the thin and thick Compton regimes.

### 5.9. Swift J1930.5+3414

This source has a counterpart classified as a galaxy in the 2MASS extended catalog (2MASX J19301380+3410495) (Kennea et al. 2005). The source is possibly detected as a radio source located  $7''$  away (NVSS J193013+341047) by the NVSS survey, with a 20 cm flux of  $3.9 \pm 0.5$  mJy and it is also likely an *IRAS* source. It has recently been classified as a Seyfert 1 galaxy at a redshift  $z = 0.0629$  (Halpern 2006) but no X-ray data have so far been reported.

The X-ray spectrum is well described (see Fig 10) by an absorbed power law with photon index frozen at 1.8 plus a power law having the same photon index but only absorbed by the Galactic column density. This extra component is required by the data with a significance  $> 99.73\%$  and accounts for excess emission below 2 keV (see Table 3). We estimate an intrinsic column density of  $\sim 3 \times 10^{23} \text{ cm}^{-2}$ , a value at odds with the Seyfert 1 classification.

In the spectrum of the optical counterpart of Swift J1930.5+3414, we confirm the emission features reported by Halpern (2006), i.e., broad (FWHM  $\sim 5800 \text{ km s}^{-1}$ ) Balmer lines with a narrow component on top and with an overall skewed profile, as well as a prominent narrow (FWHM  $\sim 900 \text{ km s}^{-1}$ ) [O III] line along with narrow [S II], [O II], [Ne III] emissions and other weaker features, all superimposed on a flat continuum (Figure 14, central left panel). The narrow emission lines are at redshift  $z = 0.063 \pm 0.001$ , in agreement with Halpern (2006). This corresponds to a luminosity distance  $D_L = 303.9 \text{ Mpc}$  and gives a 2–10 keV luminosity of  $2.0 \times 10^{43} \text{ erg s}^{-1}$  for this source. Likewise, assuming a magnitude  $B \sim 17.0$ , one gets an absolute  $B$ -band magnitude  $M_B \sim -21.2$ . This should however be considered as a conservative upper limit as no absorption local to the host galaxy was accounted for.

The  $H_\beta$ /[O III] flux ratio, 0.34, allows us to revise the Seyfert 1 AGN classification given by Halpern (2006) and to classify this object as an intermediate Seyfert of type 1.5–1.8; the absorption detected suggests that a higher Seyfert classification may be more appropriate. Furthermore, the diagnostic ratios indicate that this AGN operates in the Compton thin regime.

### 5.10. Swift J1933.9+3258

This source (Grupe et al. 2006) was first discovered as a bright X-ray source during the *ROSAT* All Sky Survey as 1RXS J193347.6+325422 (Voges et al. 1999). The object has a counterpart in the 2MASS and *IRAS* catalogs and it is also listed in the NVSS survey (NVSS J193347+325426) with a 20 cm flux of  $4.0 \pm 0.5$  mJy. The *Swift* BAT detection triggered an optical spectroscopic observation, which allowed the classification of the source as a Seyfert

1.2 galaxy at  $z = 0.0580 \pm 0.0001$  (Torres et al. 2006). Preliminary analysis of the XRT data (Grupe et al. 2006) provided a best-fit model of a broken power law with a soft photon index of  $\sim 3$ , a hard photon index of  $\sim 2$ ,  $E_B \sim 1.3$  keV and an absorption column density  $N_H \sim 3.4 \times 10^{21} \text{ cm}^{-2}$ , which is in agreement with the value found with *ROSAT* data.

Our XRT analysis, although consistent with a broken power law description, is also compatible with a simple power law model (see Fig 11) with  $\Gamma \sim 2$  (see Table 2); in either case, we do not find evidence for absorption ( $N_H < 6 \times 10^{21} \text{ cm}^{-2}$ ) in excess of the Galactic value.

The optical spectra we acquired show broad He I, He II, Fe I, and Balmer emissions ( $\text{FWHM}_{H\beta} \sim 3800 \text{ km s}^{-1}$ ) at least up to  $H_\zeta$ , as well as narrow ( $\text{FWHM} \sim 800 \text{ km s}^{-1}$ ) [O III] and [Ne III] emission lines (Figure 13, central right panel) on a blue continuum. The spectral appearance, together with a  $H_\beta$ /[O III] flux ratio ( $\sim 3.5$ ), implies a Seyfert 1.2 classification for this galaxy, in agreement with Torres et al. (2006); the redshift inferred from the optical spectrum is  $z = 0.063 \pm 0.001$ , also in agreement with Torres et al. (2006).

This gives a luminosity distance  $D_L = 284.3$  Mpc to the source, which corresponds to a luminosity of  $7.6 \times 10^{43} \text{ erg s}^{-1}$  in the 2–10 keV band and an absolute  $B$ -band magnitude  $M_B \sim -24.5$  (assuming  $B \sim 13.9$ ). The overall picture, including the value of the diagnostic ratios, is that of a “canonical” Seyfert galaxy of type 1.

### 5.11. XSS J12303–4232

This source is listed in the *RXTE* Slew Survey (XSS, Revnivtsev et al. 2004); it is associated with a bright *ROSAT* object localized with sufficient accuracy to allow its identification with an *IRAS* object (F12295–4201) that is still unclassified. A previous analysis of the XRT data suggested that the spectrum was typical of a type 1 AGN and that it contained a redshifted ( $z \sim 0.1$ ) iron line (Revnivtsev et al. 2006).

Our own analysis of individual and combined XRT data confirms the presence of a canonical AGN spectrum (see Table 2 and Figure 12); an iron line is required by the data with  $> 99\%$  confidence level ( $\Delta\chi^2 = 12$  for 2 degrees of freedom).

The *RXTE* flux of  $\sim 5 \times 10^{-12} \text{ erg cm}^{-2} \text{ s}^{-1}$  in the 3–8 keV energy band is fully compatible with the two XRT measurements.

Optical spectroscopy of the object at the XRT position shows broad Balmer, He I, He II and Fe I emissions ( $\text{FWHM}_{H\beta} \sim 5800 \text{ km s}^{-1}$ ) plus narrow [O I], [O II] and [O III], [N II], [S II], [Ne III] emission lines, detected on a flat spectral continuum (Figure 14, lower left panel);

$H_\alpha$  and  $H_\beta$  also show a narrow component on top of the broad one. The  $H_\beta/[O\text{ III}]$  flux ratio, 1.1, allows us to classify this object as a Seyfert 1.5. From the observed wavelengths of the narrow features, we determine for the first time a firm redshift for this galaxy at  $z = 0.100 \pm 0.001$ , definitely compatible with the value inferred by X-ray analysis of the iron line. The source luminosity distance is  $D_L = 495.7$  Mpc, providing a  $(9.1\text{--}15.3) \times 10^{43}$  erg s $^{-1}$  luminosity range and, assuming  $B \sim 14.3$  and no local absorption, an absolute magnitude  $M_B \sim -24.6$ .

As expected, the diagnostic ratios further confirm that this source is in the Compton thin regime.

## 6. Conclusions

We have presented optical classification and X-ray characterization of 12 hard X-ray selected objects: 11 are associated with active galaxies and only one turned out to be an Intermediate Polar (magnetic) CV at  $\sim 170$  pc from Earth (see Appendix). Optical spectroscopy allowed, for the first time, the classification of 8 objects and a distance determination for 3 of them. For another object a more refined optical classification than that available in the literature is also provided. In the 3 remaining objects, optical spectroscopy provides a characterization of the source closer in time to the X-ray measurement. Of this AGN sample, 6 objects are Seyfert 2 galaxies and 5 are Seyferts of intermediate type 1.2–1.8;  $\sim 70\%$  of the sample is absorbed with  $N_H > 10^{22}$  cm $^{-2}$ . At least 2 type 1–1.5 objects show absorption in excess of the Galactic value; particularly interesting is the case of Swift J0918.5+1618 (Mrk 704) in which the absorption is complex and may be linked to the polar scattered nature of the source. At most 3 objects (Swift J0444.1+2813, Swift J0601.9–8636 and Swift J1238.9–2720) could be Compton thick. However, in the case of Swift J0444.1+2813 and Swift J1238.9–2720 the diagnostic ratios provide controversial results: while the  $L_X/L_{OIII}$  ratio indicates a Compton thick object, two other ratios suggest a Compton thin nature. Both the upper limit on the iron line  $EW$  and the short-term variability argue against a Compton thick nature for Swift J0444.1+2813. In the case of Swift J1238.9–2720, the X-ray data analysis indicates the presence of intrinsic absorption with  $N_H \sim 5 \times 10^{23}$  cm $^{-2}$  and of a 6.4 keV iron line with an  $EW \sim 500$  eV, and suggests that we are dealing with a borderline source, heavily absorbed, but not truly Compton thick. The third source, Swift J0601.9–8636 is probably the best candidate Compton thick object in the entire sample. Overall, our findings emphasize the need for hard X-ray surveys to discover and properly sample the population of absorbed AGNs.

## 7. Acknowledgements

We thank Stefano Bernabei and Roberto Gualandi for the assistance at the telescope in Loiano, and Claudio Aguilera and Arturo Gomez for their support during observations at CTIO. This research has made use of data obtained from SIMBAD database operated at CDS, Strasbourg, France; the High Energy Astrophysics Science Archive Research Center (HEASARC), provided by NASA’s Goddard Space Flight Center; the USNO-A2.0 and 2MASS catalogs; the NASA/IPAC Extragalactic Database (NED); the ASI Scientific Data Center; and the HyperLeda catalog operated at the Observatoire de Lyon, France. This research has been supported by ASI under contracts I/008/07/0 and I/023/05.

### A. *Swift* J0732.5–1331

This is the only source in our list which is not extragalactic. It coincides in position with the Bright *ROSAT* All Sky Survey source (RASS) 1RXS J073237.6–133113 (Voges et al. 1999).

A preliminary analysis of the XRT spectrum (Ajello et al. 2006a) indicates that either a power law with photon index  $\Gamma = 1.1$ , or a Raymond-Smith model (Raymond & Smith 1977) with a temperature of 60 keV are a good fit to the data; in both cases, the hydrogen column density is below  $10^{19} \text{ cm}^{-2}$ , which implies a rather small distance from Earth. A reanalysis of the data by Wheatley, Marsh & Clarkson (2006) showed that a partial covering absorption model allows the fitted temperature to drop to a value of  $\sim 20$  keV.

Our own analysis of the XRT data are in agreement with the Wheatley, Marsh & Clarkson (2006) results, providing a best-fit model of a partially covering absorber ( $N_{\text{H}} \sim 10^{23} \text{ cm}^{-2}$  and  $C_{\text{f}} \sim 60\%$ ) plus a thermal component (MEKAL model in XSPEC, see Mewe, Gronenschild & van der Oord 1985) having an average  $kT$  of  $\sim 15$  keV (see Figure 15 and Table 3). We therefore confirm previous findings both for individual observations and for the average spectrum (see Table 3).

Masetti et al. (2006e) stressed that the *Swift* XRT error box encompasses two objects; the brighter one (with  $R \sim 12.4$ ) has the spectrum of a normal G/K-type Galactic star. The fainter one (with  $R \sim 14.2$ ), located  $\sim 10''$  southeast with respect to the brighter object, is instead the true optical counterpart: spectroscopy reveals  $\text{H}_{\alpha}$ ,  $\text{H}_{\beta}$ , He I  $\lambda 5875$  and He II  $\lambda 4686$  in emission at redshift zero, superimposed on a very blue and otherwise featureless continuum (Figure 16). These signatures are typical of the accretion disk of a Galactic X-ray binary.

Marsh et al. (2006) subsequently found that the counterpart proposed by Masetti et al. (2006e) resolves into two stars approximately  $1''.8$  apart and lying along a North-East/South-West axis, and that the actual counterpart is the northeastern star of the close pair. This star is also approximately half as bright as its companion in the  $g'$  optical filter.

After this report, optical and X-ray follow-up observations revealed a pulsation period (512.42 s, Patterson et al. 2006; Wheatley, Marsh & Clarkson (2006)) and an orbital periodicity (0.2335 d, Thorstensen et al. 2006), which suggest that this object could be classified as an Intermediate Polar (IP) magnetic Cataclysmic Variable (CV).

Indeed, the optical spectrum we obtained (Fig. 13, central left panel) shows that the  $EW$ s of He II ( $3.0 \pm 0.3$ ) Å and  $\text{H}_{\beta}$  ( $1.5 \pm 0.2$ ) Å have a ratio typical of IP CVs. In addition, the observed inverted  $\text{H}_{\alpha}/\text{H}_{\beta}$  Balmer ratio ( $\sim 2.2$ ) is often found in this class of objects; it

also suggests negligible absorption towards the source, in agreement with the X-ray data.

Considering no interstellar absorption, an absolute optical magnitude  $M_V \sim 9$  and an intrinsic color index  $(V - R)_0 \sim 0$  mag (Warner 1995) for the object, and assuming that the true counterpart contributes to roughly one third of the total  $R$  magnitude ( $R \sim 14.2$ ) from the close star pair, we derive a distance of  $\sim 190$  pc. This implies a 2–10 keV luminosity for this source of  $\sim 3.6 \times 10^{31}$  erg s $^{-1}$ .

## REFERENCES

- Ajello, M., Greiner, J., Rau, A., et al. 2006a, ATel, 697
- Ajello, M., Greiner, J., Küpcü Yoldas, A., et al. 2006b, ATel, 864
- Bassani, L., Dadina, M., Maiolino, R., Salvati, M., Risaliti, G., Della Ceca, R., Matt, G., & Zamorani, G. 1999, ApJS, 121, 473
- Bikmaev, I. F., Sunyaev, R. A., Revnivtsev, M. G., & Burenin, R. A. 2006, Astr. Letters, 32, 221
- Bird, A. J., Malizia, A., Bazzano, A., et al. 2007, ApJS, 170, 175
- Colless, M. 2003, <http://www2.aao.gov.au/2dFGRS/Public/Release/PhotCat/photcalib.html>
- Condon, J. J., Cotton, W. D., Greisen, E. W., et al. 1998, AJ, 115, 1693
- Da Costa, L. N., Willmer, C. N. A., Pellegrini, P. S., et al. 1998, AJ, 116, 1
- David, L. P., Jones, C., & Forman, W. 1992, ApJ, 388, 82
- Durret, F. 1989, A&AS, 81, 253
- Dickey, J. M., & Lockman, F. J. 1990, ARA&A, 28, 215
- Fairall, A. P. 1979, Nature, 279, 140
- Fairall, A. P. 1983, MNRAS, 203, 47
- Fisher, K. B., Huchra, J. P., Strauss, M. A., Davis, M., Yahil, A., Schlegel, D. 1995, ApJS, 100, 69
- Fouque, P., et al. 1992, Catalog of optical radial velocities, Obs. Lyon et Paris-Meudon, Vol. 1, p. 1

- Gehrels, N., Chincarini, G., Giommi, P., et al. 2004, *ApJ*, 611, 1005
- Gimeno, G. N., Díaz, R. J., & Carranza, G. J. 2004, *AJ*, 128, 62
- Grogin, N. A., Geller, M. J., & Huchra, J. P., *ApJS*, 119, 277
- Grupe, D., Tueller, J., Markwardt, C., et al. 2006, *ATel*, 859
- Halpern, J. P. 2006, *ATel*, 847
- Hambly, N. C., MacGillivray, H. T., Read, M. A., et al. 2001, *MNRAS*, 326, 1279
- Hamuy, M., Walker, A. R., Suntzeff, N. B., Gigoux, P., Heathcote, S. R., & Phillips, M. M. 1992, *PASP*, 104, 533
- Hamuy, M., Suntzeff, N. B., Heathcote, S. R., Walker, A. R., Gigoux, P., & Phillips, M. M. 1994, *PASP*, 106, 566
- Hewitt, A., & Burbidge, G. 1991, *ApJS*, 75, 297
- Hill, J. E., Burrows, D. N., Nousek, J. A., et al. 2004, *Proc. SPIE*, 5165, 21
- Ho, L. C., Filippenko, A. V., & Sargent, W. L. W. 1993, *ApJ*, 417, 63
- Ho, L. C., Filippenko, A. V., & Sargent, W. L. W. 1997, *ApJS*, 112, 315
- Hoffman, J. L., Chornock, R., Leonard, D. C., & Filippenko, A. V. 2005, *MNRAS*, 363, 1241
- Jones, D.H., Saunders, W., Colless, M., et al. 2004, *MNRAS*, 355, 747
- Kennea, J. A., Markwardt, C. B., Tueller J., et al. 2005, *ATel*, 677
- Maccacaro, T., Perola, G. C., & Elvis, M. 1982, *ApJ*, 257, 47
- Maiolino, R., Marconi, A., Salvati, M., Risaliti, G., Severgnini, P., Oliva, E., La Franca, F., & Vanzi, L. 2001, *A&A*, 365, 28
- Maiolino, R., & Rieke, G. H. 1995, *ApJ*, 454, 95
- Malizia, A., Landi, R., Bassani, L., et al. 2007, *ApJ*, in press, [[astro-ph/0706.2547](#)]
- Malizia, A., Bassani, L., Capalbi, M., Fabian, A. C., Fiore, F., & Nicastro, F. 2003, *A&A*, 406, 105
- Marsh, T. R., Littlefair, S., & Dhillon, V. S. 2006, *ATel*, 760



- Markwardt, C. B., Tueller, J., Skinner, G. K., Gehrels, N., Barthelmy, S. D., & Mushotzky, R. F. 2005, *ApJ*, 633, L77
- Masetti, N., Palazzi, E., Bassani, L., Malizia, A., & Stephen, J. B. 2004, *A&A*, 426, L41
- Masetti, N., Mason, E., Bassani, L., et al. 2006a, *A&A*, 448, 547
- Masetti, N., Pretorius, M. L., Palazzi, E., et al. 2006b, *A&A*, 449, 1139
- Masetti, N., Bassani, L., Bazzano, A., et al. 2006c, *A&A*, 455, 11
- Masetti, N., Morelli, L., Palazzi, E., Stephen, J. B., Bazzano, A., Dean, A. J., Walter, R., & Minniti, D. 2006d, *ATel*, 783
- Masetti, N., Bassani, L., Dean, A. J., Ubertini, P., & Walter, R. 2006e, *ATel*, 735
- Mauch, T., Murphy, T., Buttery, H. J., Curran, J., Hunstead, R. W., Piestrzynski, B., Robertson, J. G., Sadler, E. M. 2003, *MNRAS*, 342, 1117
- Mewe, R., Gronenschild, E. H. B. M., & van den Oord, G. H. J. 1985, *A&AS*, 62, 197
- Monet, A. K. B., Levine, S. E., Monet, D. G., Bowell, E. L. G., Koehn, B., & Bryan, B. 1999, *BAAS*, 31, 1532
- Morelli, L., Masetti, N., Bassani, L., Landi, R., Malizia, A., Bird, A. J., Ubertini, P., Galaz, G., 2006, *ATel*, 785
- Moretti, A., Campana, S. Tagliaferri, G., et al. 2004, *Proc. SPIE* 5165, 232
- Mulchaey, J. S., Koratkar, A., Ward, M. J., Wilson, A. S., Whittle, M., Antonucci, R. R. J., Kinney, A. L., & Hurt, T. 1994, *ApJ*, 436, 586
- Nagao, T., Taniguchi, Y., & Murayama, T. 2000, *AJ*, 119, 2605
- Ohashi T., et al. 1996, *PASJ*, 48, 157
- Osterbrock, D. E. 1989, *Astrophysics of Gaseous Nebulae and Active Galactic Nuclei* (Mill Valley: Univ. Science Books)
- Panessa, F., & Bassani, L. 2002, *A&A*, 394, 435
- Pantoja, C. A., Altschuler, D. R.; Giovanardi, C., & Giovanelli, R. 1997, *AJ*, 113, 905
- Patterson, J., Halpern, J., Mirabal, N., et al. 2006, *ATel*, 757

- Piconcelli, E., Sànchez-Portal, M., Guainazzi, M., et al. 2006, *A&A*, 453, 839
- Quadrelli, A., Malizia, A., Bassani, L., & Malaguti, G. 2003, *A&A*, 411, 77
- Raymond, J. C., & Smith, B. W. 1977, *ApJS*, 35, 419
- Revnivtsev, M. G., Sazonov, S. Yu., Jahoda, K., & Gilfanov, F. 2004, *A&A*, 418, 927
- Revnivtsev, M. G., Sazonov, S., Churazov, E., & Trudolyubov, S. 2006, *A&A*, 448, L49
- Risaliti, G. 2002, *A&A*, 386, 379
- Risaliti, G., Maiolino, R., & Salvati, M. 1999, *ApJ*, 522, 157
- Sanders, D. B., Mazzarella, J. M., Kim, D.-C., Surace, J. A., & Soifer, B. T. 2003, *AJ*, 126, 1607
- Sazonov, S. Yu. & Revnivtsev, M. G. 2004, *A&A*, 423, 469
- Schlegel, D. J., Finkbeiner, D. P., & Davis, M. 1998, *ApJ*, 500, 525
- Schwope, A., Hasinger, G., Lehmann, I., et al. 2000, *Astron. Nachr.*, 321, 1
- Skrutskie, M. F., Cutri, R. M., Stiening, R., et al. 2006, *AJ*, 131, 1163
- Smith, J. E., Robinson, A., Alexander, D. M., Young, S., Axon, D. J., & Corbett, E. A. 2004, *MNRAS*, 350, 140
- Stone, R. P. S. 1977, *ApJ*, 218, 767
- Thorstensen, J. R., Patterson, J., Halpern, J., & Mirabal, N. 2006, *ATel*, 767
- Torres, M. A. P., Steeghs, D., Garcia, M. R., et al. 2006, *ATel*, 862
- Tueller, J., Barthelmy, S., Burrows, D., et al. 2005, *ATel*, 669
- Turner, T. J., George, I. M., Nandra, K., & Mushotzky, R. F. 1997, *ApJ*, 488, 164
- Ueda, Y., Eguchi S., Terashima, Y., et al. 2007, [[astro-ph/0706.1168](#)]
- Veilleux, S., & Osterbrock, D. E. 1987, *ApJS*, 63, 295
- Voges, W., et al. 1999, *A&A*, 349, 389
- Warner, B. 1995, *Cataclysmic variable stars* (Cambridge: Cambridge Univ. Press)
- Weingartner, J. C., & Murray, N. 2002, *ApJ*, 580, 88

Wheatley, P. J., Marsh, T. R., & Clarkson, W. 2006, ATel, 765

White, R. L., Becker, R. H., Helfand, D. J., & Gregg, M. D. 1997, ApJ, 475, 479

Winkler, H. 1992, MNRAS, 257, 677

Winkler, H., & Payne, P. 1990, South African Astron. Obs. Circ., 14, 21

Zombeck, M. V. 1990, Handbook of Space Astronomy and Astrophysics

Table 1. Log of the *Swift* XRT observations presented in this paper.

Source	R.A. (J2000)	Dec (J2000)	Error (arcsec)	Obs date	Exposure (s)	Energy band (keV)	Count rate ( $10^{-3}$ counts $s^{-1}$ )
Swift J0444.1+2813	04 44 09.23	+28 12 58.62	3.53	Aug 02, 2005	7206	–	–
Swift J0444.1+2813				Aug 04, 2005	4759	–	–
Swift J0444.1+2813				Aug 11, 2005	6637	–	–
Swift J0444.1+2813				Aug 20, 2005	12793	1.0–8.5	$74.5 \pm 2.6$
Swift J0444.1+2813				Dec 05, 2005	29205	1.0–9.3	$96.3 \pm 1.8$
Swift J0444.1+2813				Dec 06, 2005	24567	1.0–8.0	$80.4 \pm 1.8$
Swift J0444.1+2813				Dec 07, 2005	24124	1.0–8.2	$87.2 \pm 1.9$
Swift J0601.9–8636	06 05 39.24	–86 37 51.32	4.57	Dec 14, 2005	10211	0.5–5.0	$1.80 \pm 0.50$
Swift J0601.9–8636				Dec 18, 2005	2477	–	–
Swift J0601.9–8636				Dec 20, 2005	700	–	–
Swift J0732.5–1331	07 32 37.70	–13 31 06.18	4.74	Jan 06, 2006	3445	0.5–6.4	$125.3 \pm 6.2$
Swift J0732.5–1331				Jan 06, 2006	332	–	–
Swift J0732.5–1331				Apr 27, 2006	4044	0.5–6.4	$136.6 \pm 5.8$
Swift J0732.5–1331				Oct 03, 2006	4763	0.5–6.4	$146.3 \pm 6.8$
Swift J0823.4–0457	08 23 00.93	–04 56 04.01	4.17	Jan 06, 2006	1239	2.0–6.0	$9.7 \pm 2.5$
Swift J0823.4–0457				Oct 16, 2006	5362	2.0–6.0	$13.1 \pm 1.5$
Swift J0823.4–0457				Oct 21, 2006	4763	2.0–6.0	$15.3 \pm 1.8$
Swift J0918.5+1618				Jan 06, 2006	673	–	–
Swift J0918.5+1618	09 18 25.95	+16 18 20.05	3.56	Jun 14, 2006	2258	0.7–6.4	$352.6 \pm 12.6$
Swift J0918.5+1618				Sep 28, 2006	5602	0.7–6.5	$212.1 \pm 6.5$
Swift J0918.5+1618				Jan 21, 2007	1750	0.7–7.0	$294.5 \pm 13.1$
Swift J1009.3–4250	10 09 48.12	–42 48 42.60	4.00	Jun 15, 2006	1809	0.5–6.5	$11.5 \pm 2.7$
Swift J1009.3–4250				Jul 11, 2006	3877	0.5–7.5	$13.8 \pm 2.0$
Swift J1009.3–4250				Jul 13, 2006	1964	0.5–7.5	$11.5 \pm 2.5$
Swift J1009.3–4250				Jul 28, 2006	6180	0.2–7.5	$18.4 \pm 1.8$
Swift J1009.3–4250				Jul 30, 2006	0.91	–	–
Swift J1038.8–4942	10 38 44.87	–49 46 52.73	3.56	Oct 26, 2005	5225	1.0–7.5	$114.7 \pm 4.7$
Swift J1038.8–4942				Nov 05, 2005	3852	1.0–7.0	$90.2 \pm 4.8$
Swift J1038.8–4942				Dec 22, 2005	17112	1.0–8.0	$81.0 \pm 2.2$
Swift J1200.8+0650	12 00 57.74	06 48 21.04	3.64	Dec 11, 2005	15055	2.0–7.5	$36.3 \pm 1.6$
Swift J1200.8+0650				Dec 21, 2005	3287	1.5–6.0	$37.6 \pm 3.5$
Swift J1238.9–2720	12 38 54.58	–27 18 27.45	3.83	Jun 15, 2005	8610	1.5–7.5	$18.9 \pm 1.6$
Swift J1238.9–2720				Aug 15, 2005	2385	2.0–7.5	$20.4 \pm 3.2$
Swift J1238.9–2720				Aug 28, 2005	11527	2.0–8.0	$17.0 \pm 1.3$
Swift J1930.5+3414	19 30 13.70	34 10 52.74	4.15	Dec 12, 2005	3792	–	–
Swift J1930.5+3414				Dec 15, 2005	7363	1.0–9.0	$11.8 \pm 1.4$
Swift J1930.5+3414				Dec 21, 2005	1312	–	–
Swift J1933.9+3258	19 33 47.15	32 54 25.33	3.54	Jul 07, 2006	1552	0.5–6.5	$470.8 \pm 19.5$
Swift J1933.9+3258				Oct 13, 2006	5861	0.5–7.0	$424.7 \pm 8.6$
Swift J1933.9+3258				Oct 15, 2006	4372	0.5–7.0	$446.4 \pm 10.2$
XSS J12303–4232	12 32 12.09	–42 17 50.37	3.53	Sep 08, 2005	15171	0.2–7.5	$155.6 \pm 3.5$
XSS J12303–4232				Sep 12, 2005	16333	0.2–7.5	$111.8 \pm 2.7$

Table 2. XRT spectral analysis results of sources fitted with an absorbed power law.  
Frozen parameters are written between squared brackets.

Source	$N_{\text{H Gal}}^a$	$N_{\text{H}}^a$	$\Gamma$	Flux <sup>b</sup> (2–10 keV)	$\chi^2/\nu$	$N_{\text{H}}^{a,c}$
Swift J0601.9–8636 (# 1)	0.111	–	[1.8]	$0.05 \pm 0.01$	3.8/3	–
Swift J0823.4–0457 (# 1)	0.0515	–	[1.8]	$4.2 \pm 1.1$	0.1/2	$25.2^{+49.1}_{-25.2}$
Swift J0823.4–0457 (# 2)	0.0515	–	[1.8]	$5.3 \pm 0.6$	4.1/4	$24.6^{+13.6}_{-10.7}$
Swift J0823.4–0457 (# 3)	0.0515	–	[1.8]	$5.8 \pm 0.7$	2.4/4	$33.1^{+14.9}_{-11.2}$
Swift J0823.4–0457 (all)	0.0515	–	[1.8]	$4.6 \pm 0.7$	7.8/13	$29.7^{+9.0}_{-7.5}$
Swift J0918.5+1618 (# 2)	0.0344	$< 0.3$	$1.80^{+0.11}_{-0.08}$	$13.3 \pm 0.4$	31.4/34	–
Swift J0918.5+1618 (# 3)	0.0344	$0.21^{+0.12}_{-0.10}$	$1.87^{+0.20}_{-0.18}$	$8.8 \pm 0.3$	38.0/39	$0.18^{+0.06}_{-0.08}$
Swift J0918.5+1618 (# 4)	0.0344	$< 0.12$	$1.92^{+0.21}_{-0.19}$	$10.0 \pm 0.4$	22.2/26	$< 0.1$
Swift J0918.5+1618 (2+3+4)	0.0344	$0.13^{+0.06}_{-0.07}$	$1.89^{+0.12}_{-0.13}$	$13.8 \pm 0.8$	98.2/97	$0.10^{+0.03}_{-0.05}$
Swift J1038.8–4942 (# 1)	0.272	$0.89^{+0.38}_{-0.33}$	$1.25^{+0.30}_{-0.29}$	$11.7 \pm 0.5$	26.7/27	$1.50^{+0.24}_{-0.20}$
Swift J1038.8–4942 (# 2)	0.272	$0.59^{+0.47}_{-0.38}$	$1.41^{+0.42}_{-0.38}$	$8.4 \pm 0.4$	8.3/14	$1.20^{+0.25}_{-0.22}$
Swift J1038.8–4942 (# 3)	0.272	$0.50^{+0.17}_{-0.16}$	$1.16^{+0.16}_{-0.10}$	$7.8 \pm 0.2$	29.8/40	$1.10^{+0.13}_{-0.14}$
Swift J1038.8–4942 (all)	0.272	$0.50^{+0.14}_{-0.13}$	$1.21^{+0.15}_{-0.14}$	$9.3 \pm 0.4$	91.0/106	$1.28^{+0.12}_{-0.10}$
Swift J1200.8+0650 (# 1)	0.0144	$6.50^{+2.50}_{-1.92}$	$1.26^{+0.62}_{-0.53}$	$5.7 \pm 0.2$	27.7/24	$8.08^{+0.23}_{-0.98}$
Swift J1200.8+0650 (# 2)	0.0144	$7.94^{+8.53}_{-4.62}$	$1.87^{+2.58}_{-1.67}$	$5.4 \pm 0.5$	11.8/11	$7.65^{+2.35}_{-1.64}$
Swift J1200.8+0650 (all)	0.0144	$6.61^{+2.17}_{-1.78}$	$1.31^{+0.58}_{-0.51}$	$5.8 \pm 0.3$	40.0/37	$8.30^{+1.10}_{-0.90}$
Swift J1933.9+3258 (# 1)	0.226	$< 0.04$	$2.05^{+0.14}_{-0.12}$	$14.4 \pm 0.6$	35.5/36	$< 0.02$
Swift J1933.9+3258 (# 2)	0.226	$< 0.01$	$2.05^{+0.07}_{-0.06}$	$13.5 \pm 0.3$	75.8/81	$< 0.01$
Swift J1933.9+3258 (# 3)	0.226	$< 0.01$	$2.15^{+0.08}_{-0.06}$	$12.6 \pm 0.3$	77.3/68	$< 0.01$
Swift J1933.9+3258 (all)	0.226	$< 0.04$	$2.08^{+0.05}_{-0.04}$	$13.8 \pm 0.4$	192.8/186	$< 0.02$

Note. — <sup>a</sup> In units of  $10^{22} \text{ cm}^{-2}$ ;  
<sup>b</sup> In units of  $10^{-12} \text{ erg cm}^{-2} \text{ s}^{-1}$ ;  
<sup>c</sup> Assuming a photon index  $\Gamma = 1.8$ ;

Table 3. XRT spectral analysis results of sources requiring more complex models. Frozen parameters are written between squared brackets.

Source	$N_{\text{H,Gal}}^a$	$N_{\text{H}}^a$	$C_f$	$\Gamma$ (keV)	$E_{\text{line}}$ (eV)	$EW$ (keV)	$kT$ (2–10 keV)	Flux <sup>b</sup>	$\chi^2/\nu$	$N_{\text{H}}^{a,c}$
Swift J0444.1+2813 (# 4)	0.196	$4.76^{+1.30}_{-1.42}$	—	$1.32^{+0.35}_{-0.36} d$	—	—	—	$10.0 \pm 0.4$	48.5/49	$6.37^{+0.93}_{-0.74}$
Swift J0444.1+2813 (# 5)	0.196	$4.08^{+0.62}_{-0.44}$	—	$1.53^{+0.20}_{-0.14} d$	—	—	—	$12.0 \pm 0.2$	95.1/119	$4.81^{+0.36}_{-0.26}$
Swift J0444.1+2813 (# 6)	0.196	$4.31^{+0.82}_{-0.74}$	—	$1.42^{+0.22}_{-0.19} d$	—	—	—	$10.0 \pm 0.3$	97.6/113	$5.40^{+0.50}_{-0.40}$
Swift J0444.1+2813 (# 7)	0.196	$4.21^{+0.90}_{-0.83}$	—	$1.41^{+0.24}_{-0.19} d$	—	—	—	$11.0 \pm 0.3$	89.1/89	$5.49^{+0.50}_{-0.45}$
Swift J0444.1+2813 (all)	0.196	$4.25^{+0.42}_{-0.32}$	—	$1.46^{+0.11}_{-0.09} d$	—	—	—	$10.7 \pm 0.3$	341.4/376	$5.35^{+0.65}_{-0.23}$
Swift J0732.5–1331 (# 1)	—	$13.0^{+12.7}_{-6.4}$	$0.68^{+0.15}_{-0.32}$	—	—	—	$13.0^{+66.0}_{-7.5}$	$10.2 \pm 0.4$	12.4/21	—
Swift J0732.5–1331 (# 3)	—	$5.1^{+5.4}_{-2.2}$	$0.61^{+0.14}_{-0.23}$	—	—	—	$9.8^{+64.7}_{-4.3}$	$9.6 \pm 0.4$	32.2/24	—
Swift J0732.5–1331 (# 4)	—	$16.0^{+16.2}_{-8.2}$	$0.65^{+0.15}_{-0.26}$	—	—	—	$21.9^{+57.0}_{-13.9}$	$12.1 \pm 0.5$	24.4/21	—
Swift J0732.5–1331 (all)	—	$11.6^{+6.3}_{-4.5}$	$0.63^{+0.10}_{-0.19}$	—	—	—	$15.4^{+56.5}_{-5.91}$	$12.0 \pm 0.4$	73.7/72	—
Swift J1009.3–4250 (# 1)	0.109	—	—	[1.8] <sup>d</sup>	—	—	—	$1.9 \pm 0.4$	2.8/4	$21.7^{+195.5}_{-15.5}$
Swift J1009.3–4250 (# 2)	0.109	—	—	[1.8] <sup>d</sup>	—	—	—	$1.5 \pm 0.2$	12.5/16	$14.3^{+10.4}_{-5.6}$
Swift J1009.3–4250 (# 3)	0.109	—	—	[1.8] <sup>d</sup>	—	—	—	$1.9 \pm 0.4$	3.8/5	$45.7^{+55.6}_{-21.5}$
Swift J1009.3–4250 (# 4)	0.109	$45.8^{+9.5}_{-10.7}$	—	$2.50^{+0.70}_{-0.40} d$	—	—	—	$2.8 \pm 0.3$	23.0/20	$41.4^{+12.1}_{-8.8}$
Swift J1009.3–4250 (all)	0.109	$39.8^{+10.8}_{-9.6}$	—	$2.32^{+0.58}_{-0.62} d$	—	—	—	$2.0 \pm 0.3$	48.7/44	$36.2^{+8.6}_{-7.2}$
Swift J1238.9–2720 (# 1)	0.0668	—	—	[1.8]	$6.48^{+0.10}_{-0.13}$	$528^{+313}_{-295}$	—	$4.4 \pm 0.4$	18.6/13	$41.2^{+10.5}_{-8.0}$
Swift J1238.9–2720 (# 2)	0.0668	—	—	[1.8]	$6.46^{+0.20}_{-0.10}$	$632^{+600}_{-546}$	—	$5.4 \pm 0.8$	6.8/9	$81.0^{+51.3}_{-14.3}$
Swift J1238.9–2720 (# 3)	0.0668	—	—	[1.8]	$6.36^{+0.10}_{-0.07}$	$432^{+269}_{-232}$	—	$4.2 \pm 0.3$	14.6/19	$48.5^{+15.2}_{-16.5}$
Swift J1238.9–2720 (all)	0.0668	—	—	[1.8]	$6.40^{+0.07}_{-0.06}$	$508^{+174}_{-200}$	—	$4.7 \pm 0.5$	46.5/42	$46.3^{+9.6}_{-7.8}$
Swift J1930.5+3414 (# 2)	0.172	—	—	[1.8] <sup>d</sup>	—	—	—	$1.8 \pm 0.2$	10.4/17	$28.5^{+18.3}_{-11.2}$
XSS J12303–4232 (# 1)	0.0726	—	—	$1.69^{+0.06}_{-0.04}$	$6.38^{+0.08}_{-0.14}$	$331^{+219}_{-203}$	—	$5.4 \pm 0.1$	98.8/109	—
XSS J12303–4232 (# 2)	0.0726	—	—	$1.80^{+0.06}_{-0.04}$	$6.51^{+0.07}_{-0.10}$	$360^{+210}_{-203}$	—	$5.6 \pm 0.1$	99.8/108	—
XSS J12303–4232 (all)	0.0726	—	—	$1.76^{+0.03}_{-0.04}$	$6.42^{+0.07}_{-0.04}$	$343^{+115}_{-176}$	—	$5.4 \pm 0.1$	208.0/219	—

Note. — <sup>a</sup> In units of  $10^{22} \text{ cm}^{-2}$ ;

<sup>b</sup> In units of  $10^{-12} \text{ erg cm}^{-2} \text{ s}^{-1}$ ;

<sup>c</sup> Assuming a photon index  $\Gamma = 1.8$ ;

<sup>d</sup> In this case the best-fit model requires a second power law component, having the same photon index of the primary absorbed power law, and passing only through the Galactic column density.

Table 4. *ASCA* spectral analysis results of Swift J0918.5+1618 = Mrk 704.

Energy band (keV)	Count rate ( $10^{-3}$ counts s $^{-1}$ )	$N_{\text{HGal}}^a$	$N_{\text{H}}^a$	$Cf$	$\Gamma$	$E_{line}$ (keV)	$EW$ (eV)	Flux $^b$ (2–10 keV)	$\chi^2/\nu$
1.2–10.0	$66.8 \pm 1.1$	0.0344	$13.5^{+4.9}_{-3.4}$	$0.64^{+0.10}_{-0.05}$	$1.55^{+0.19}_{-0.16}$	$6.39^{+0.15}_{-0.14}$	$233^{+111}_{-112}$	$5.6 \pm 0.1$	193.7/191

Note. —  $^a$  In units of  $10^{22}$  cm $^{-2}$ ;  
 $^b$  In units of  $10^{-12}$  erg cm $^{-2}$  s $^{-1}$ .

Table 5. Log of the optical spectroscopic observations presented in this paper.

Source	Date	Telescope	Mid-exposure time (UT)	Grism or grating	Slit (arcsec)	Exposure time (s)
Swift J0444.1+2813	01 Feb 2006	1.5m Loiano	18:07:00	#4	2.0	2×900
Swift J0601.9–8636	22 Mar 2006	1.5m CTIO	00:06:53	#13/I	1.5	900
Swift J0732.5–1331	10 Feb 2006	1.5m Loiano	21:43:16	#4	2.0	2×1800
Swift J0823.4–0457	09 Feb 2006	1.5m Loiano	22:16:12	#4	2.0	2×1800
Swift J0918.5+1618	07 Feb 2006	1.5m Loiano	22:42:45	#4	2.0	2×1200
Swift J1009.3–4250	25 Mar 2004	4m AAT	11:25:22	580V	6.7	1200
Swift J1009.3–4250	25 Mar 2004	4m AAT	12:29:07	425R	6.7	600
Swift J1038.8–4942	22 Mar 2006	1.5m CTIO	02:24:02	#13/I	1.5	2×600
Swift J1200.8+0650	10 Feb 2006	1.5m Loiano	01:25:50	#4	2.0	2×1800
Swift J1238.9–2720	23 Mar 2006	1.5m CTIO	01:46:56	#13/I	1.5	2×1200
Swift J1930.5+3414	05 Aug 2006	1.5m Loiano	00:13:45	#4	2.0	2×1800
Swift J1933.9+3258	28 Jul 2006	1.5m Loiano	01:08:14	#4	2.0	2×900
XSS J12303–4232	04 Apr 2006	1.5m CTIO	00:47:38	#13/I	1.5	2×900



Table 6. Fluxes of  $H_\alpha$ ,  $H_\beta$ ,  $[O\text{ III}]$  and  $[N\text{ II}]$  emission lines detected in the spectra of the objects reported in Figures 14 and 15. Measurements and upper limits are reported at  $1\sigma$  and  $3\sigma$  confidence levels, respectively. For the extragalactic objects the values are corrected for Galactic reddening assuming a color excess,  $E(B - V)_{\text{Gal}}$ , as per Schlegel et al. (1998) and which is reported in the Table as well as the optical ( $A_{V_{\text{opt}}}$ ) and X-ray ( $A_{V_X}$ ) extinctions.

Source	$F_{H_\alpha}^a$	$F_{H_\beta}^a$		$F_{[OIII]}^a$	$F_{[NII]}^a$	$E(B - V)_{\text{Gal}}$	$A_{V_{\text{opt}}}$	$A_{V_X}^\dagger$	Type
		Broad	Narrow						
Swift J0444.1+2813	$7.4 \pm 0.7$	—	$<0.1$	$4.4 \pm 0.7$	$11.0 \pm 1.1$	0.856	$>10$	19–24	Seyfert 2 <sup>b</sup>
Swift J0601.9–8636	$1.57 \pm 0.18$	—	$<0.041$	$<0.5$	$1.52 \pm 0.18$	0.140	$>8.1$	$<0.5$	Seyfert 2 <sup>b</sup>
Swift J0732.5–1331	$1.0 \pm 0.1$	$4.4 \pm 0.5^d$		—	—	—	—	—	IP CV <sup>b,c</sup>
Swift J0823.4–0457	$1.90 \pm 0.13$	—	$0.31 \pm 0.09$	$2.0 \pm 0.1$	$1.56 \pm 0.10$	0.046	2.4	134	Seyfert 2 <sup>b</sup>
Swift J0918.5+1618	*	$15.4 \pm 0.8$	$1.15 \pm 0.12$	$7.2 \pm 0.5$	*	0.029	—	$>4.5$	Seyfert 1.2
Swift J1009.3–4250	$2.4 \pm 0.1$	—	$0.60 \pm 0.05$	$9.0 \pm 0.1$	$3.30 \pm 0.13$	0.167	1.1	163–179	Seyfert 2
Swift J1038.8–4942	*	$18.3 \pm 1.3^d$		$11.1 \pm 0.6$	*	0.496	—	2–6	Seyfert 1.5 <sup>b</sup>
Swift J1200.8+0650	$1.17 \pm 0.12$	—	$<0.25$	$0.58 \pm 0.04$	$0.42 \pm 0.06$	0.017	$>1.6$	30–37	Seyfert 2 <sup>b</sup>
Swift J1238.9–2720	$1.61 \pm 0.16$	—	$<0.07$	$1.59 \pm 0.11$	$1.43 \pm 0.14$	0.072	$>6.4$	208	Seyfert 2 <sup>b</sup>
Swift J1930.5+3414	*	$8.5 \pm 1.3$	$2.7 \pm 0.4$	$33 \pm 1$	*	0.187	—	128	Seyfert 1.5–1.8
Swift J1933.9+3258	*	$92 \pm 12^d$		$26 \pm 2$	*	0.271	—	$<0.1$	Seyfert 1.2
XSS J12303–4232	*	$20 \pm 2$	$2.2 \pm 0.2$	$20 \pm 1$	*	0.104	—	—	Seyfert 1.5 <sup>b</sup>

Note. — <sup>a</sup> In units of  $10^{-14}$  erg cm<sup>-2</sup> s<sup>-1</sup>;

<sup>b</sup> This source has been classified in this work for the first time;

<sup>c</sup> IP CV (Intermediate Polar (magnetic) Cataclysmic Variable);

<sup>d</sup> Sum of the fluxes of broad and narrow components;

\* In this case  $[N\text{ II}]$  and  $H_\alpha$  are heavily blended;

<sup>†</sup> This value has been obtained using the conversion  $A_{V_X} \simeq \frac{N_H}{2.22 \times 10^{21}}$  (Zombeck 1990)

Table 7. Hard X-ray and infrared fluxes, and diagnostics luminosity ratios.

Source	$F_{\text{HX}}^{a,b}$ (10–100 keV)	$F_{\text{IR}}^b$	$L_{\text{X}}/L_{[\text{OIII}]}$	$L_{\text{X}}/L_{\text{IR}}$	$L_{[\text{OIII}]} / L_{\text{IR}}$	$L_{\text{X}}/L_{\text{HX}}$
Swift J0444.1+2813	6.9 <sup>1</sup>	8.3	<0.008	0.13	>16.9	0.16
Swift J0601.9–8636	3.7 <sup>1</sup>	42.90	–	0.00012	–	0.001
Swift J0823.4–0457 <sup>c</sup>	2.7 <sup>2</sup>	<7.17	17.5	≤0.06	>0.0033	0.16
Swift J0918.5+1618	2.7 <sup>1</sup>	8.16	109	0.096	0.0009	0.29
Swift J1009.3–4250	2.5 <sup>3</sup>	–	7.4	–	–	0.08
Swift J1038.8–4942	3.4 <sup>1</sup>	–	83.8	–	–	0.27
Swift J1200.8+0650	2.6 <sup>1</sup>	<3.6	<200	0.16	>0.0008	0.22
Swift J1238.9–2720	12.4 <sup>1</sup>	5.7	<0.39	0.08	>0.21	0.04
Swift J1930.5+3414	2.5 <sup>1</sup>	<6.5	5.5	>0.028	>0.0051	0.07
Swift J1933.9+3258	2.7 <sup>4</sup>	6.4	30.4	0.12	0.0041	0.29
XSS J12303–4232 <sup>†</sup>	0.61	4.2	24.0	0.11	0.0047	0.89

Note. — <sup>a</sup> References: (1) BAT AGN catalog (available at <http://www.astro.umd.edu/~lwinter/research/AGN.html>); (2) Aiello et al. 2006a; (3) Ajello et al. 2006b; (4) Grupe et al. 2006;

<sup>b</sup> In units of  $10^{-11}$  erg cm<sup>−2</sup> s<sup>−1</sup>;

<sup>c</sup> Assuming that IRAS 08205–0446 is associated with Fairall 272;

<sup>†</sup> For this source we consider the *RXTE* 8–20 keV flux.

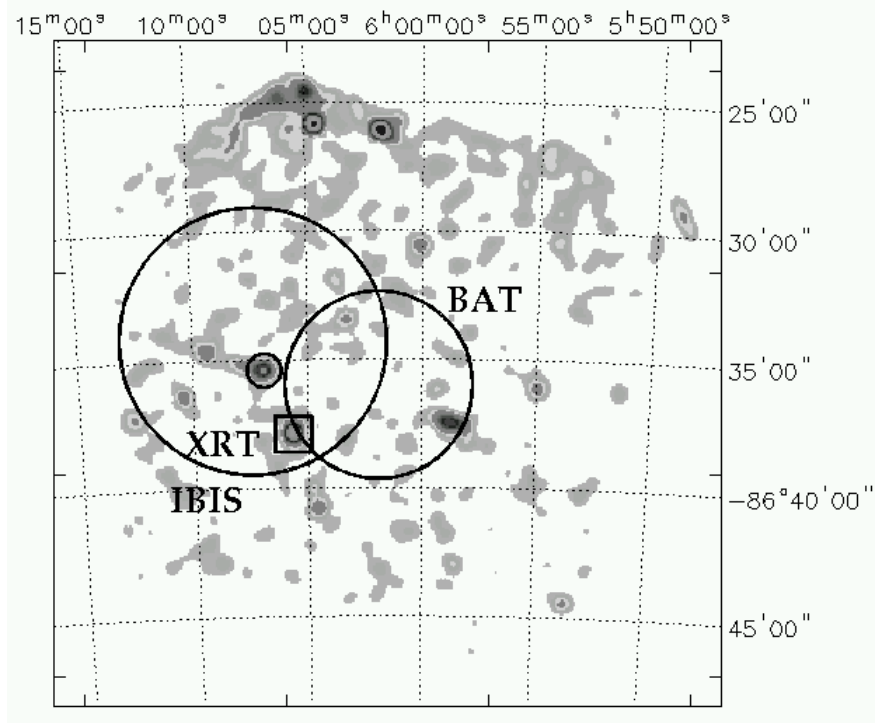


Fig. 1.— XRT field of view of the region surrounding Swift J0601.9–8636. The two large circles represent the *INTEGRAL* IBIS (left) and *Swift* BAT (right) error boxes, while the XRT position of the source is given by the small box. The smaller circle shows instead the position of the other object detected nearby and classified as a normal star.

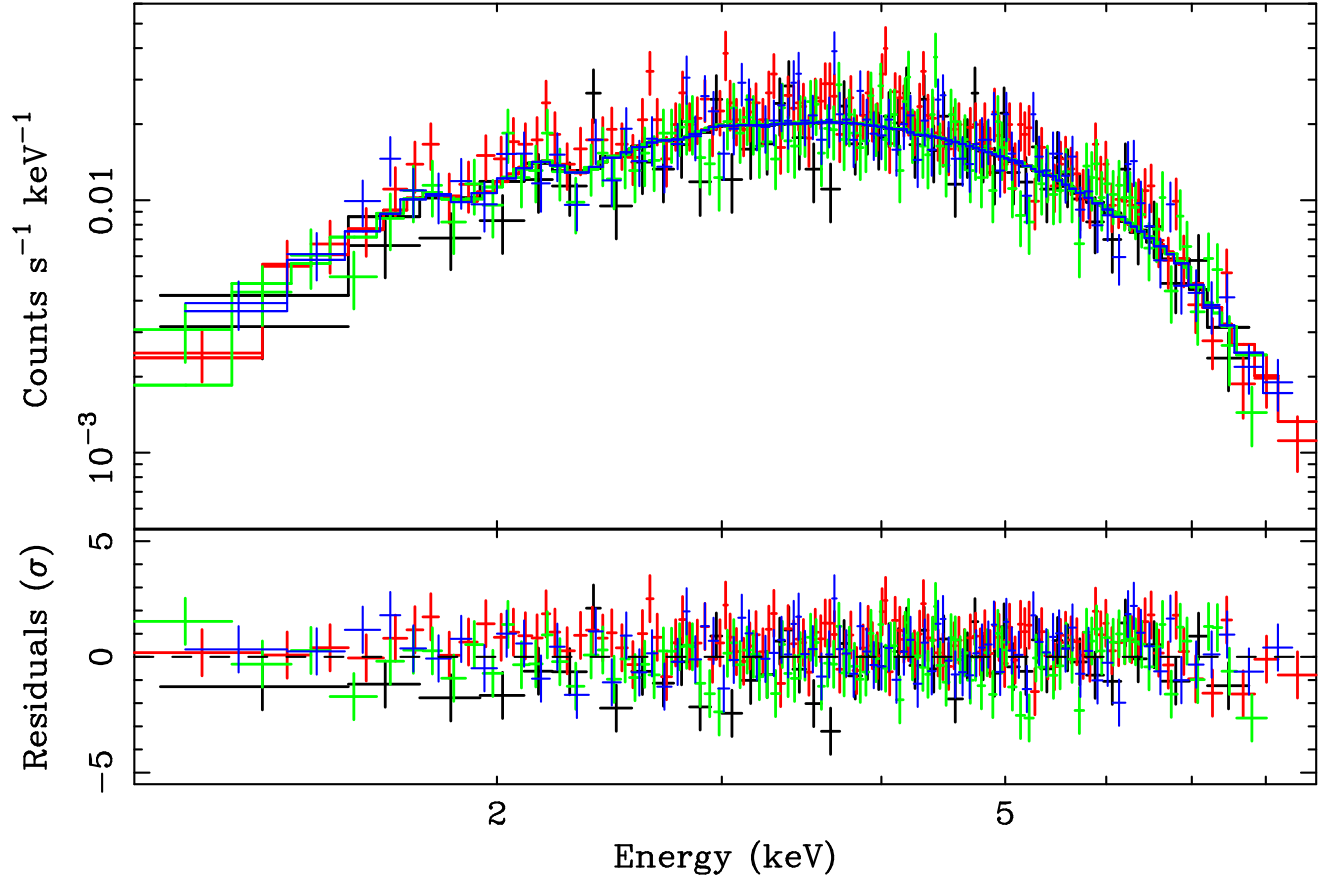


Fig. 2.— Four XRT spectra of Swift J0444.1+2813 fitted with a primary absorbed power law component plus a power law, having the same photon index, and absorbed only by Galactic column density (upper panel); residuals to this model in units of  $\sigma$  (lower panel).

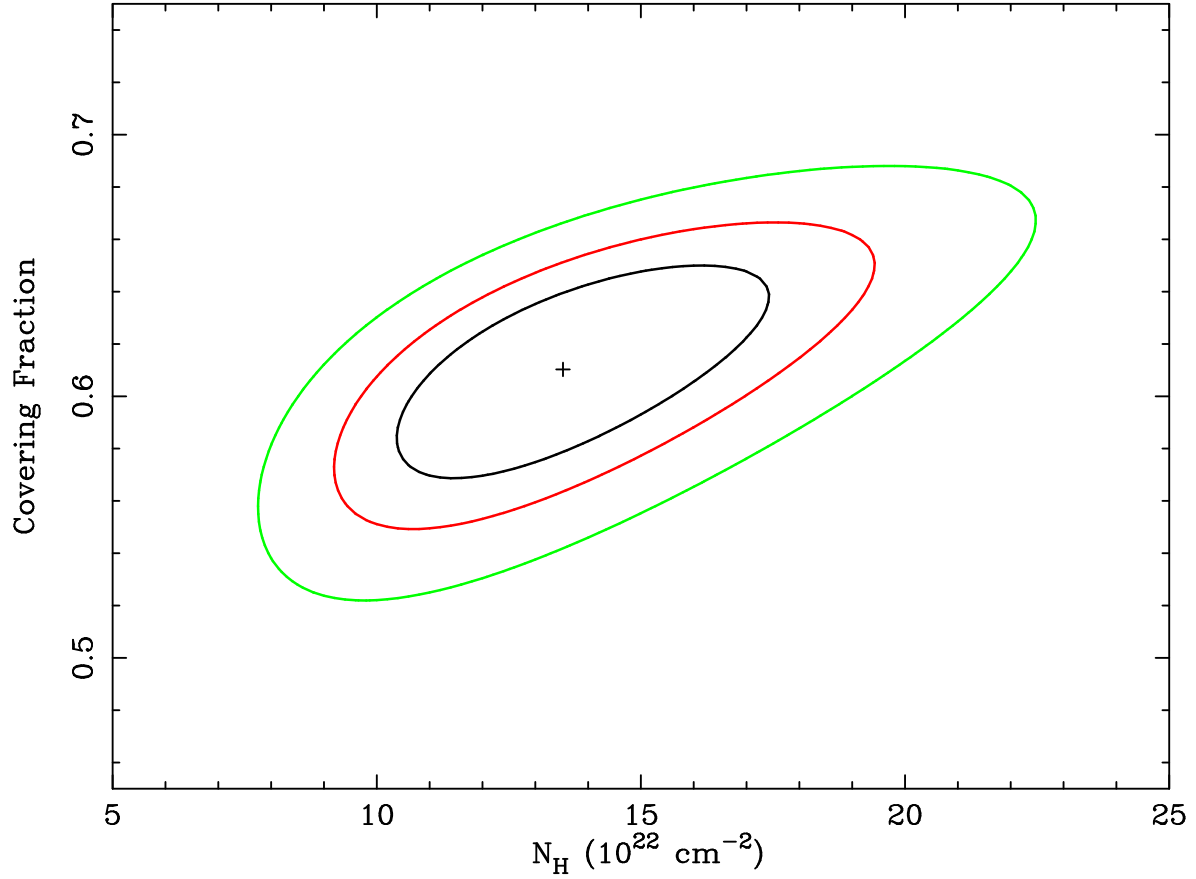


Fig. 3.— Confidence contours (at 68%, 90%, and 99% confidence level) of the covering fraction versus column density for the best-fit model used in the *ASCA* observation of Swift J0918.5+1618.

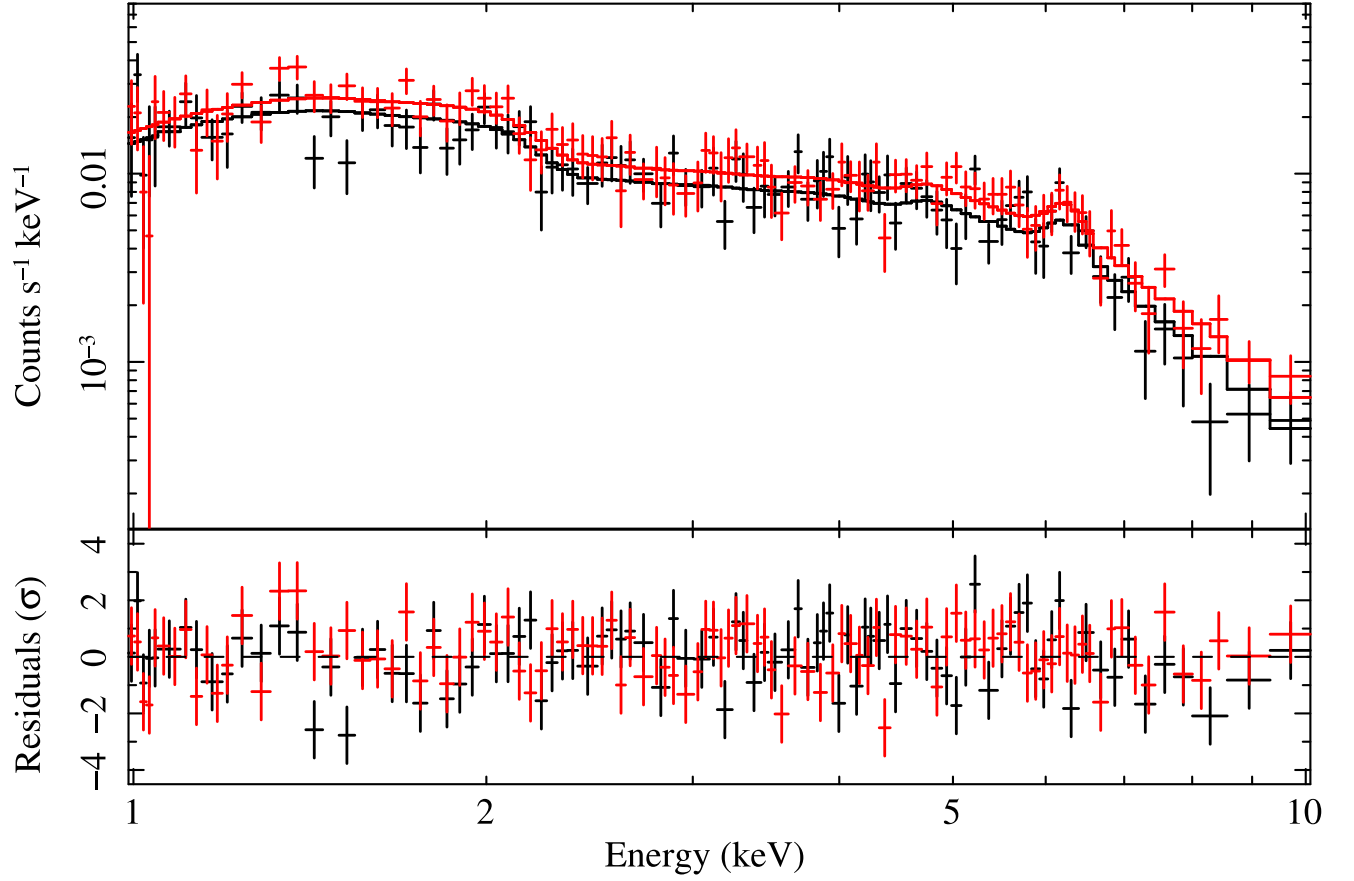


Fig. 4.— *ASCA* GIS spectra of Swift J0918.5+1618 fitted with a power law absorbed by a partially covering absorber plus a Gaussian narrow Fe  $K\alpha$  line (upper panel); residuals to this model in units of  $\sigma$  (lower panel).

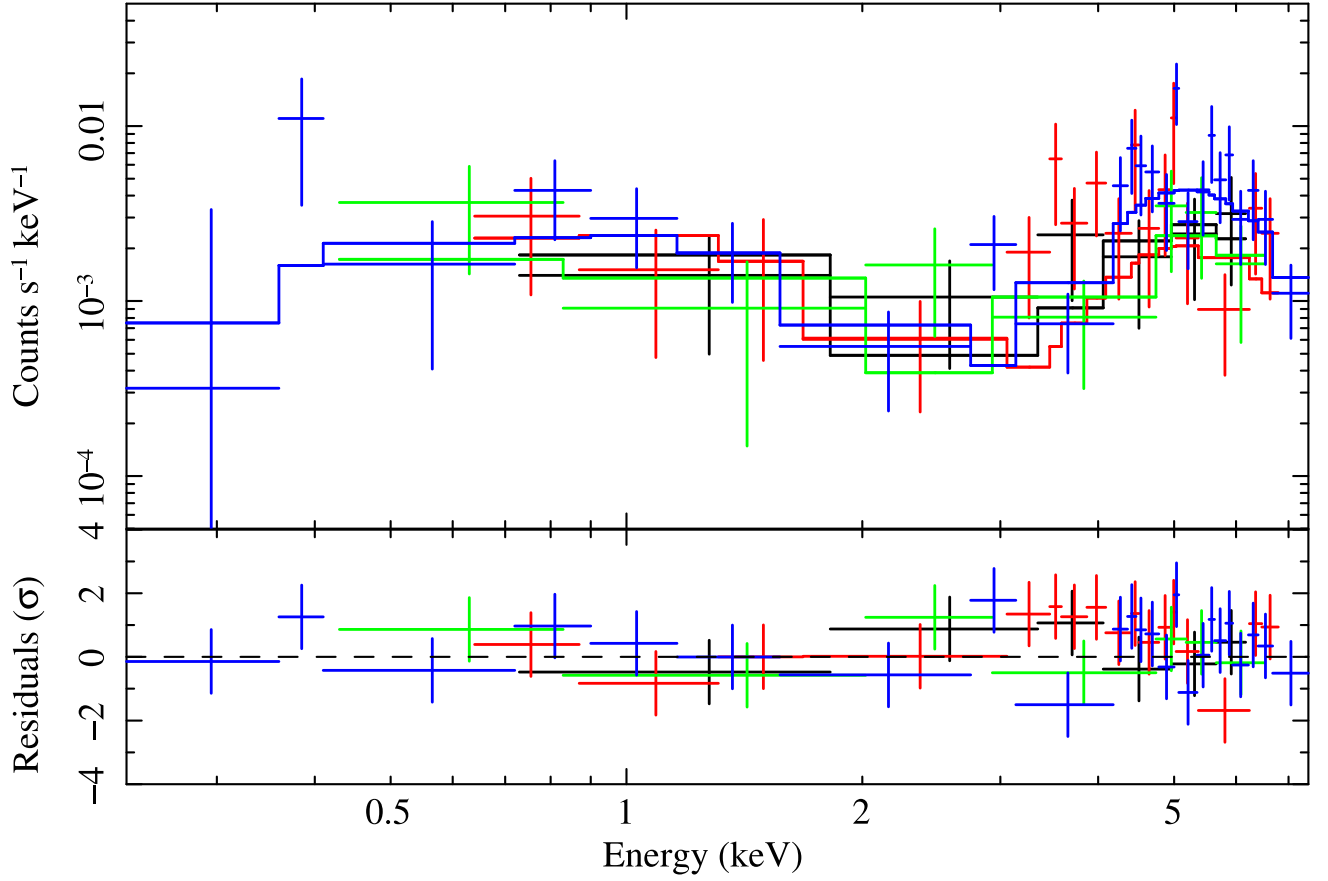


Fig. 5.— Four XRT spectra of Swift J1009.3–4250 fitted with a primary absorbed power law component plus a power law, having the same photon index, but absorbed only by Galactic column density (upper panel); residuals to this model in units of  $\sigma$  (lower panel).

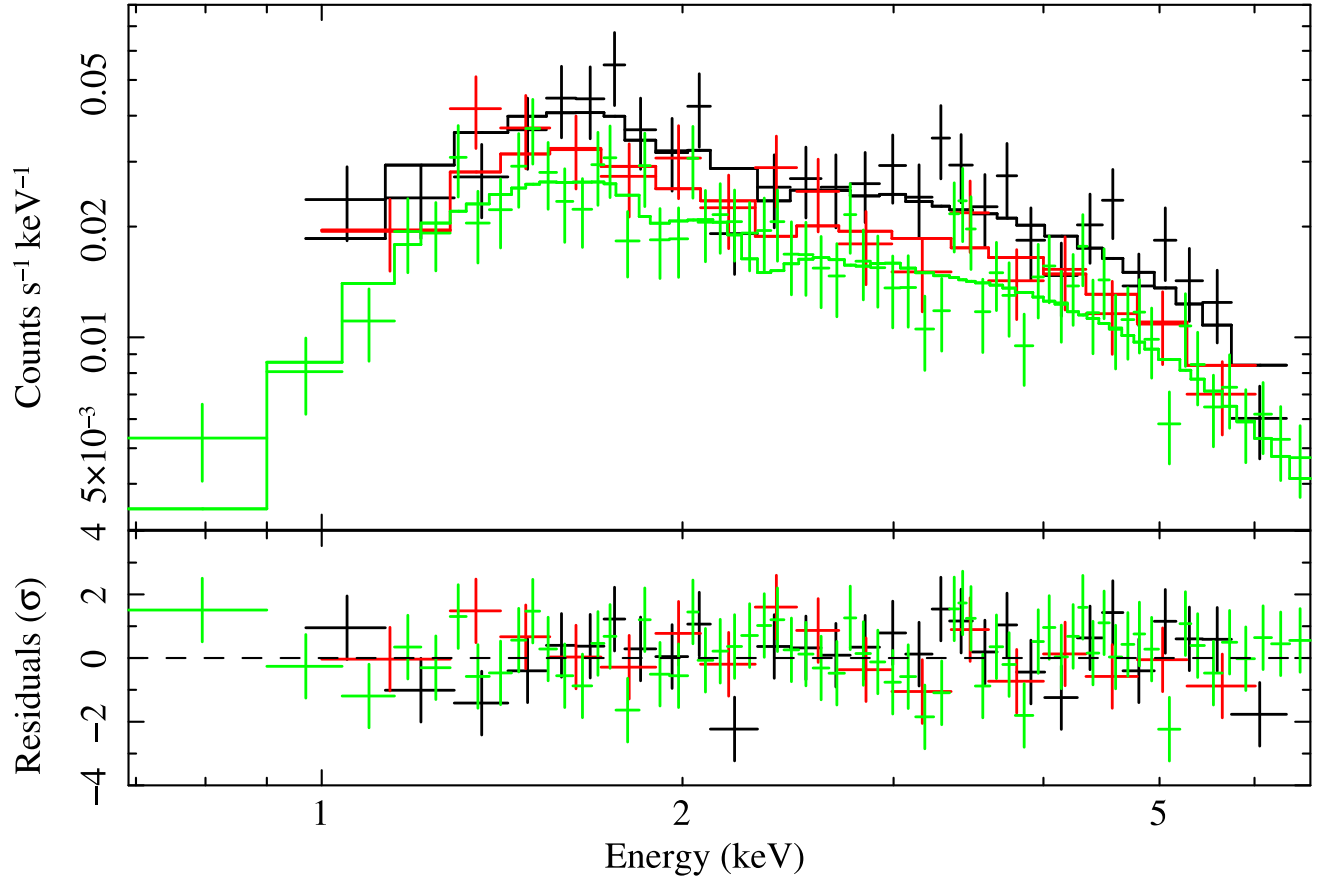


Fig. 6.— Three XRT spectra of Swift J1038.8–4942 fitted with an absorbed power law (upper panel); residuals to this model in units of  $\sigma$  (lower panel).



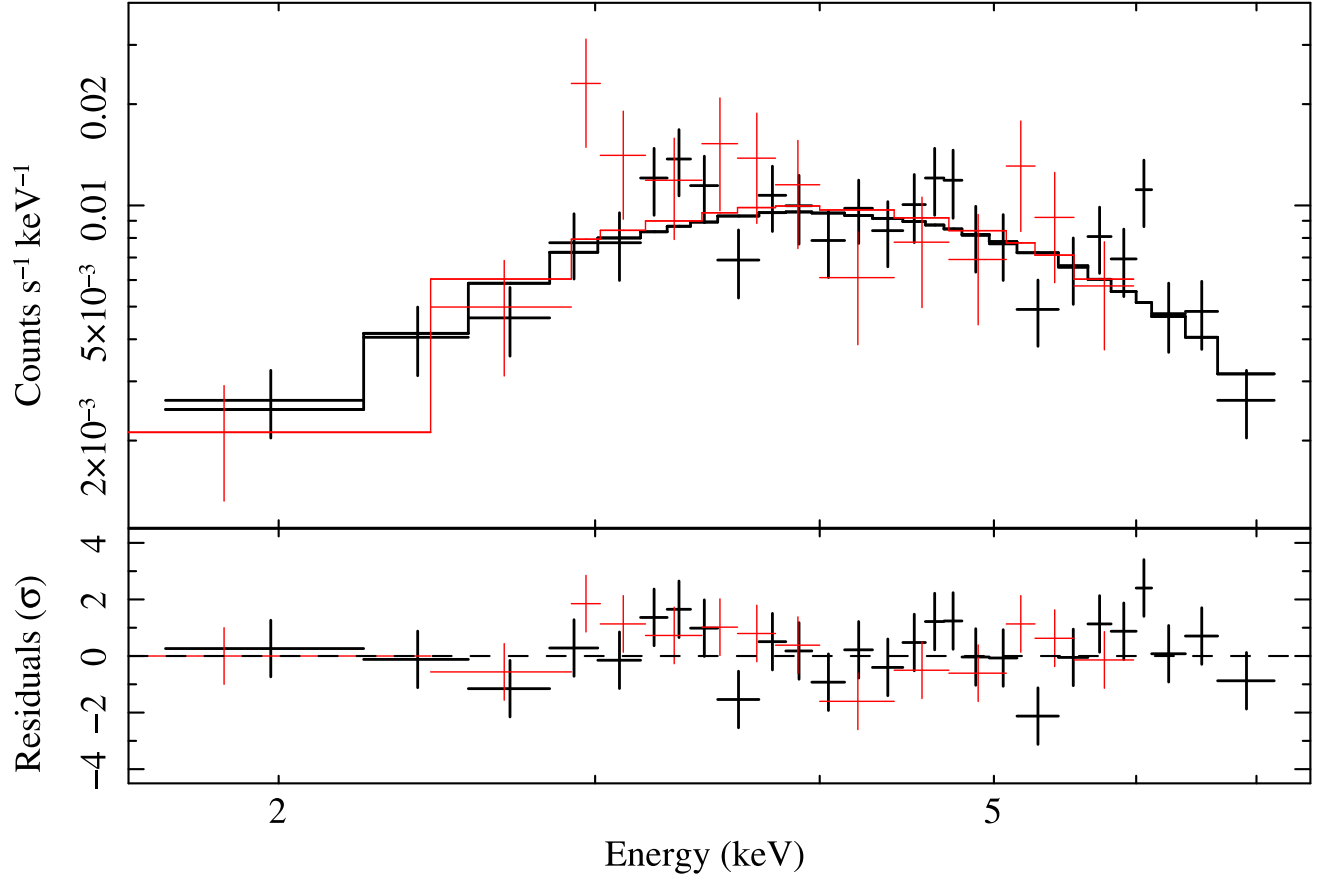


Fig. 7.— Two XRT spectra of Swift J1200.8+0650 fitted with an absorbed power law (upper panel); residuals to this model in units of  $\sigma$  (lower panel).

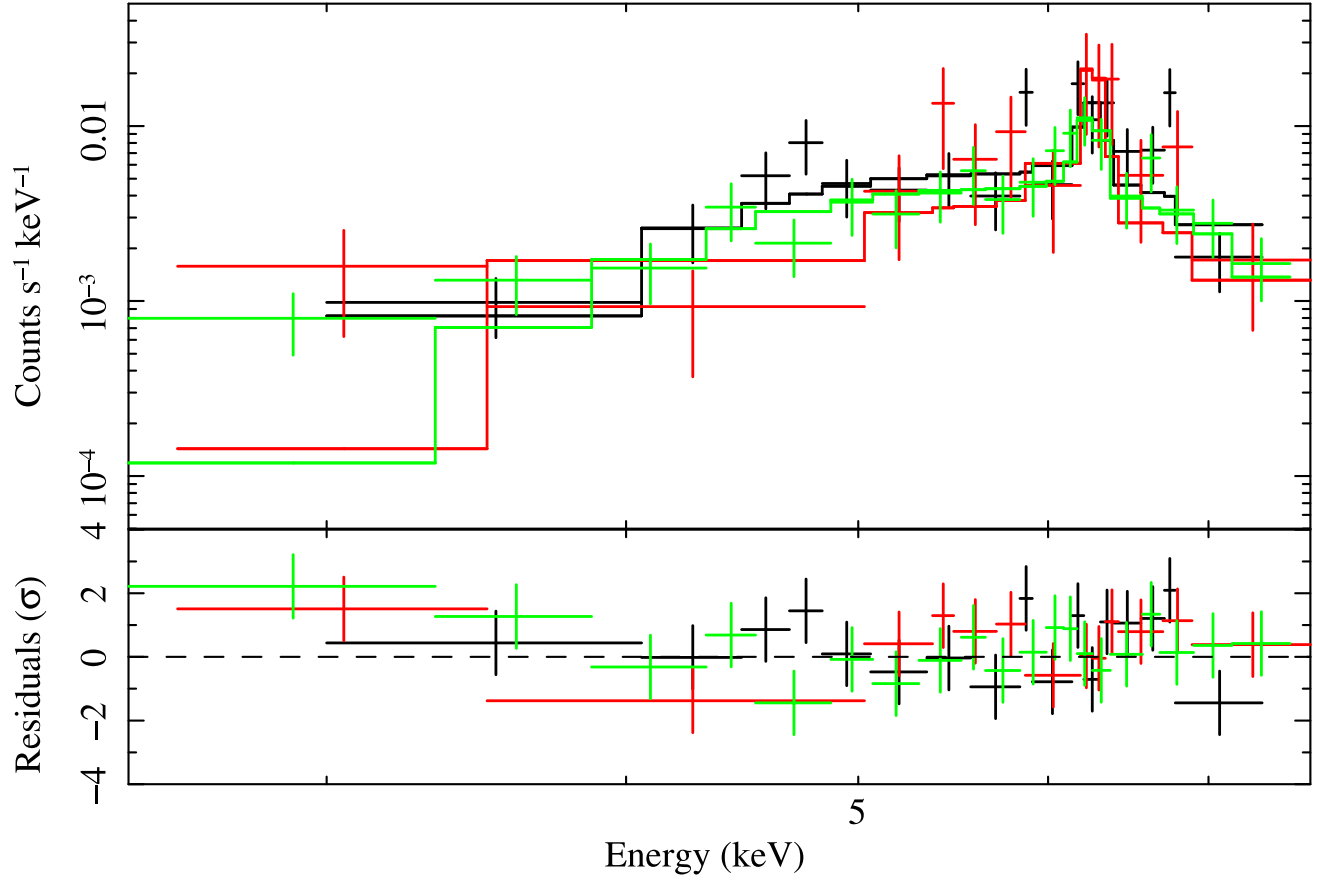


Fig. 8.— Three XRT spectra of Swift J1238.9–2720 fitted with an absorbed power law plus a narrow Gaussian Fe  $K\alpha$  line (upper panel); residuals to this model in units of  $\sigma$  (lower panel).

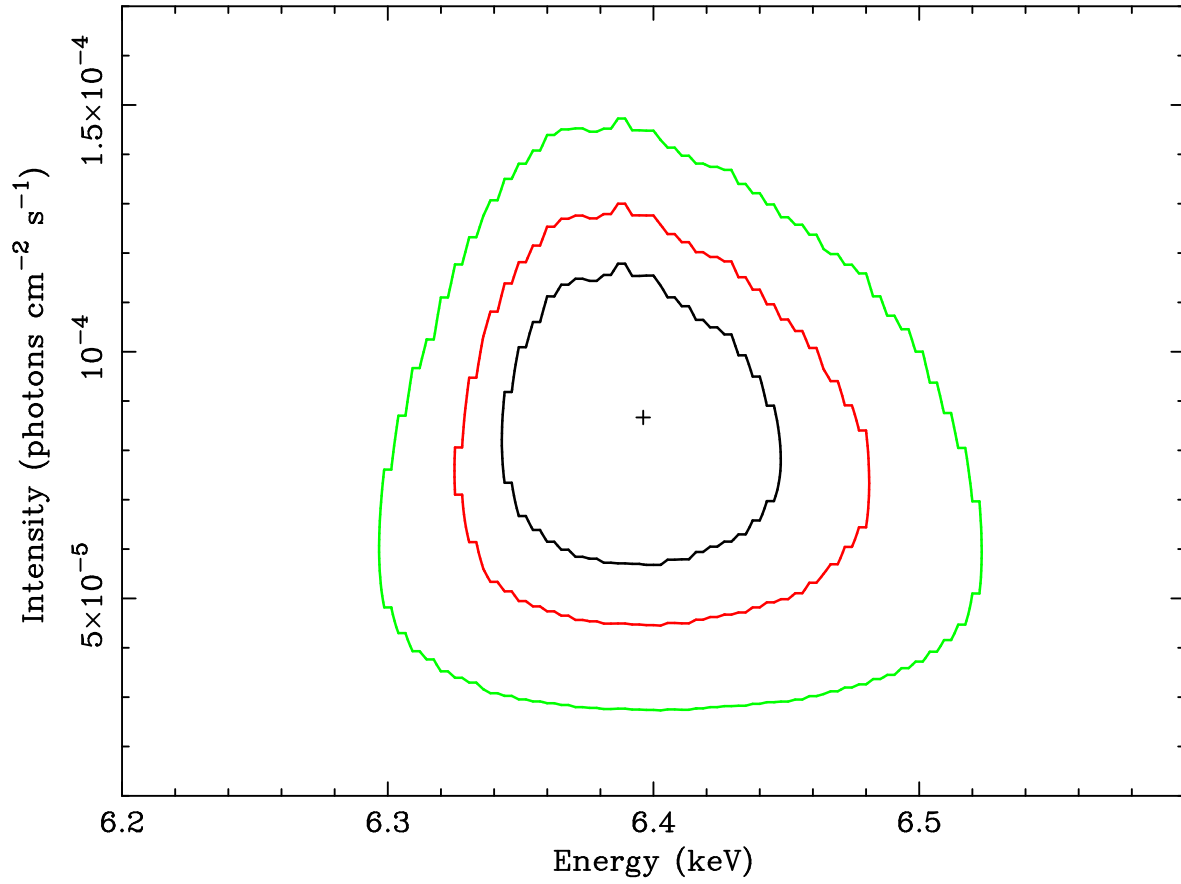


Fig. 9.— Confidence contours (at 68%, 90%, and 99% confidence level) of the iron line energy versus intensity for the best-fit model of Swift J1238.9–2720.

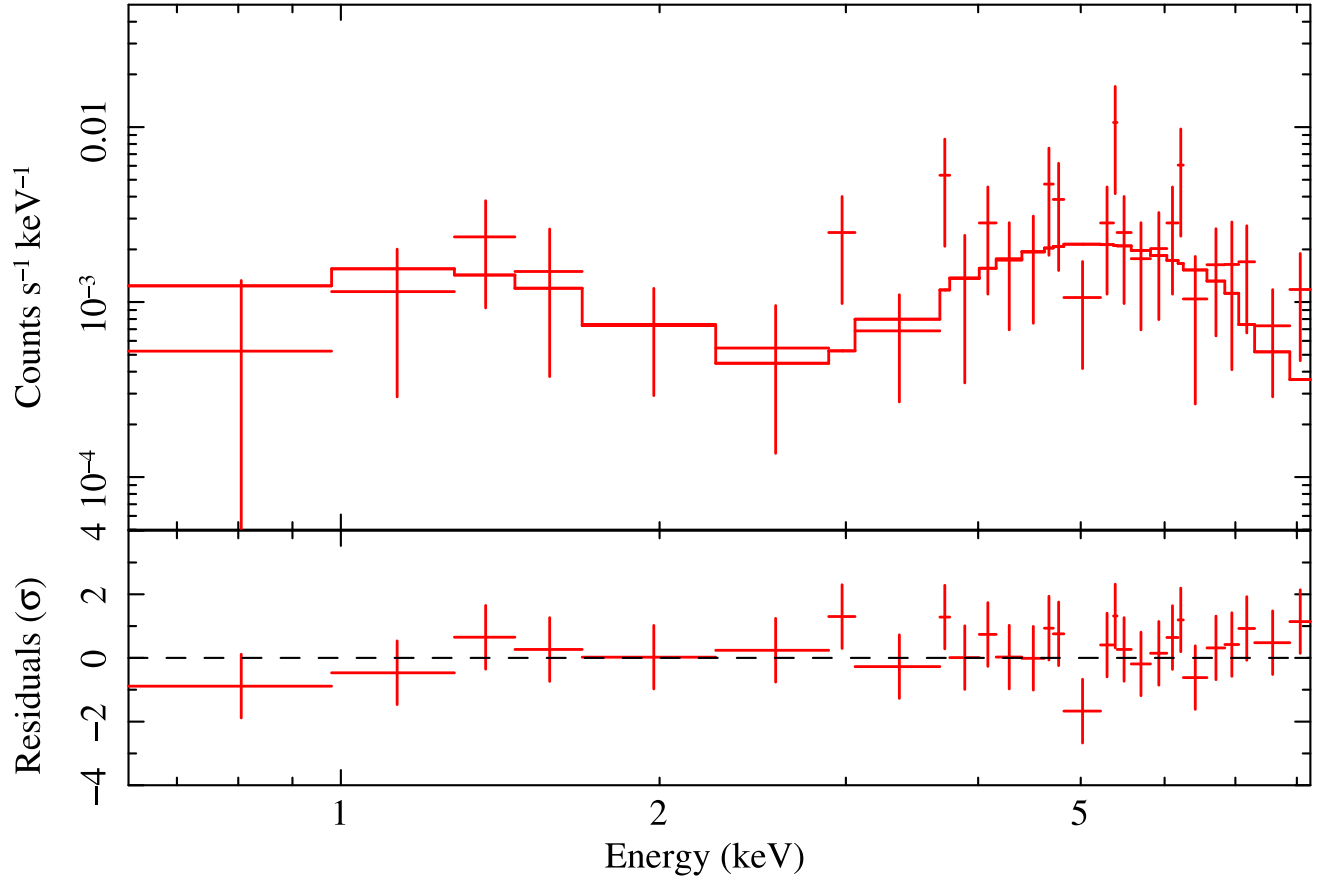


Fig. 10.— XRT spectrum (obs 2) of Swift J1930.5+3414 fitted with an absorbed power law component plus a power law, having the same photon index, but absorbed only by Galactic column density (upper panel); residuals to this model in units of  $\sigma$  (lower panel).

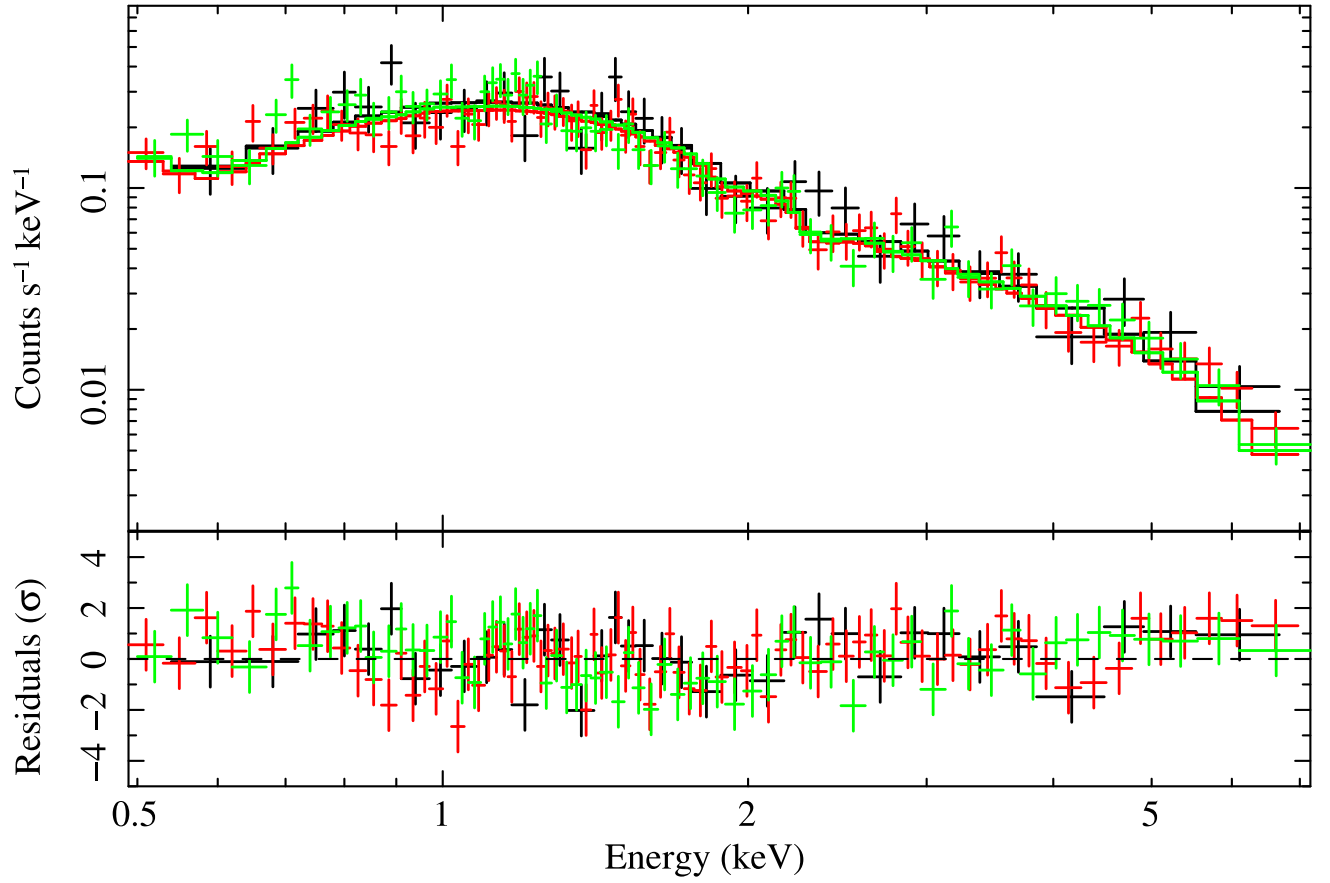


Fig. 11.— Three XRT spectra of Swift J1933.9+3258 fitted with an absorbed power law (upper panel); residuals to this model in units of  $\sigma$  (lower panel).

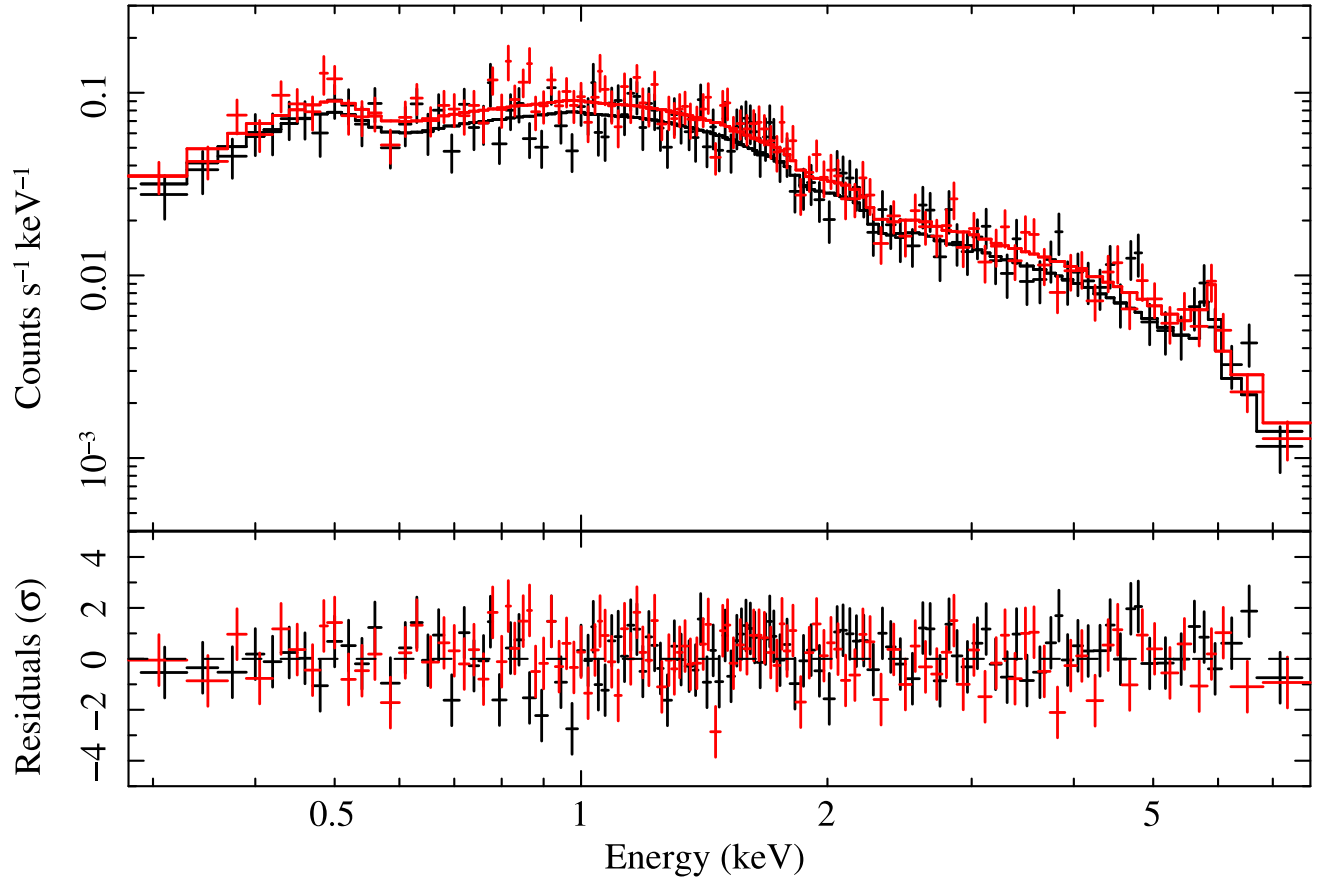


Fig. 12.— Two XRT spectra of XSS J12303–4232 fitted with an absorbed power law plus a narrow Gaussian Fe K $\alpha$  line (upper panel); residuals to this model in units of  $\sigma$  (lower panel).

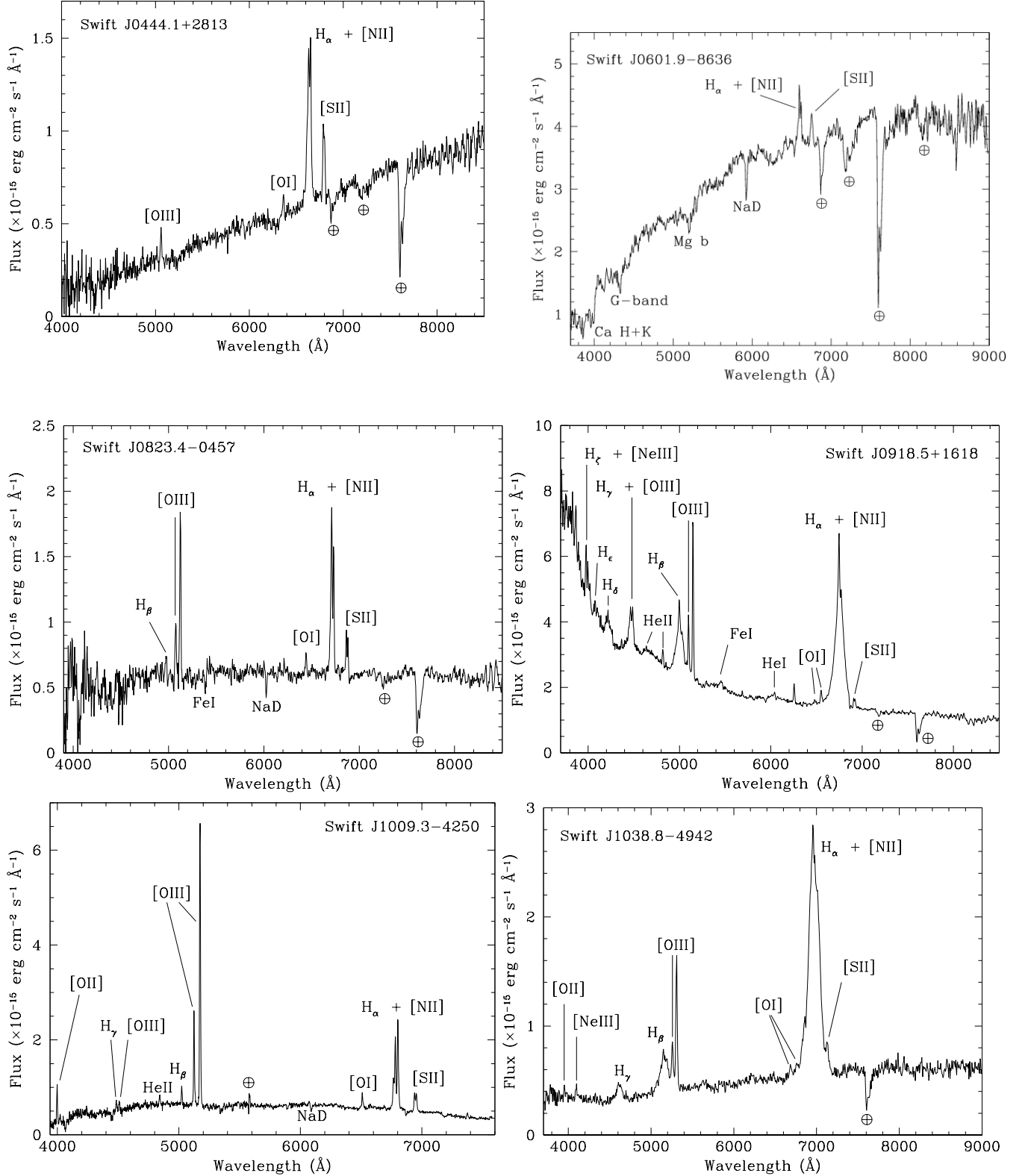


Fig. 13.— Spectra (not corrected for the intervening Galactic absorption) of the optical counterparts of Swift J0444.1+2813 (upper left panel), Swift J0601.9-8636 (upper right panel), Swift J0823.4-0457 (central left panel), Swift J0918.5+1618 (central right panel), Swift J1009.3-4250 (lower left panel) and Swift J1038.8-4942 (lower right panel). For each spectrum the main spectral features are labeled. The symbol  $\oplus$  indicates atmospheric and telluric features.

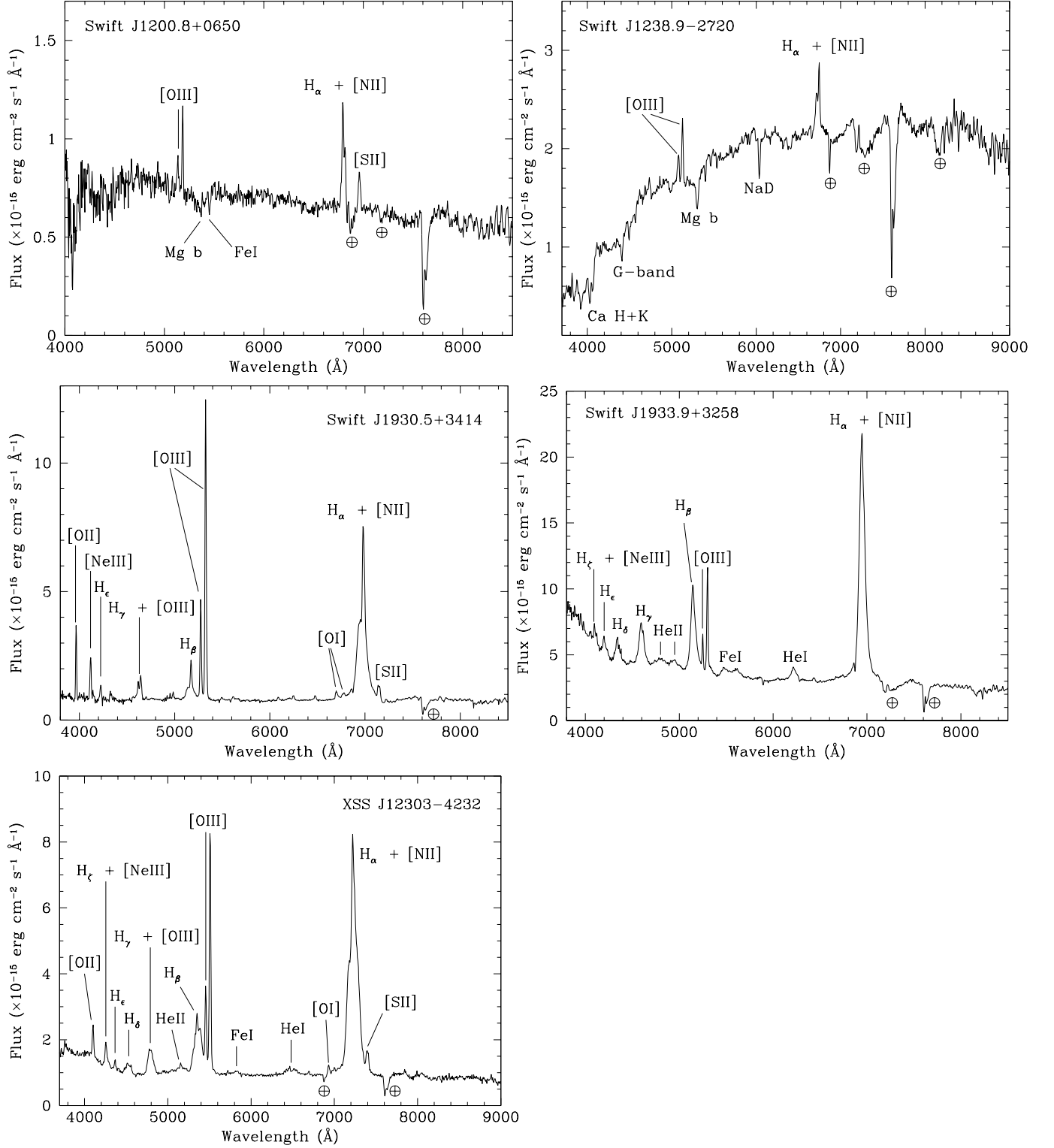


Fig. 14.— As Figure 13, but for objects Swift J1200.8+0650 (upper left panel), Swift J1238.9–2720 (upper right panel), Swift J1930.5+3414 (central left panel), Swift J1933.9+3258 (central right panel) and XSS J12303–4232 (lower left panel).



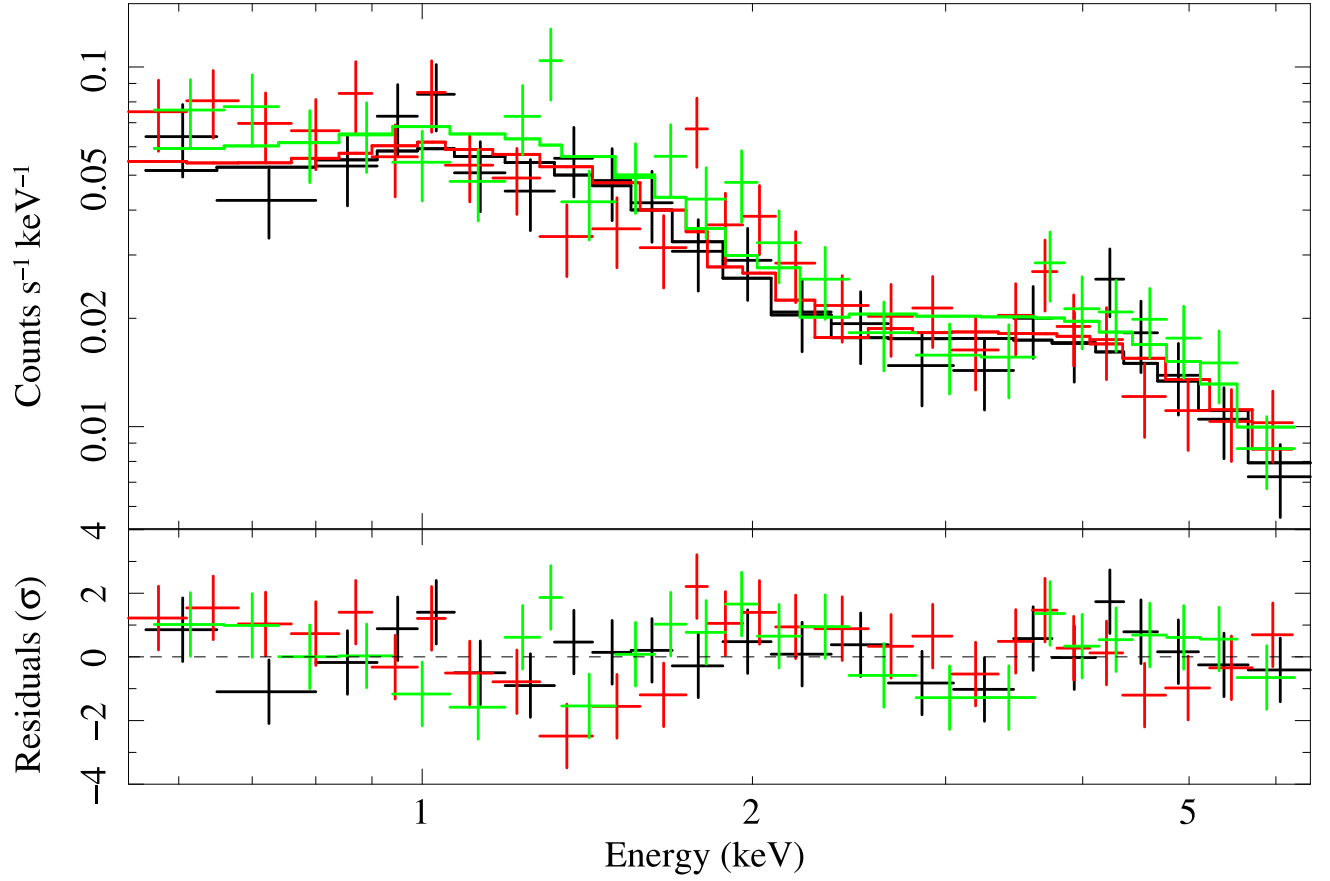


Fig. 15.— Three XRT spectra of Swift J0732.9–1331 fitted with a thermal component (MEKAL) partially absorbed (upper panel); residuals to this model in units of  $\sigma$  (lower panel).

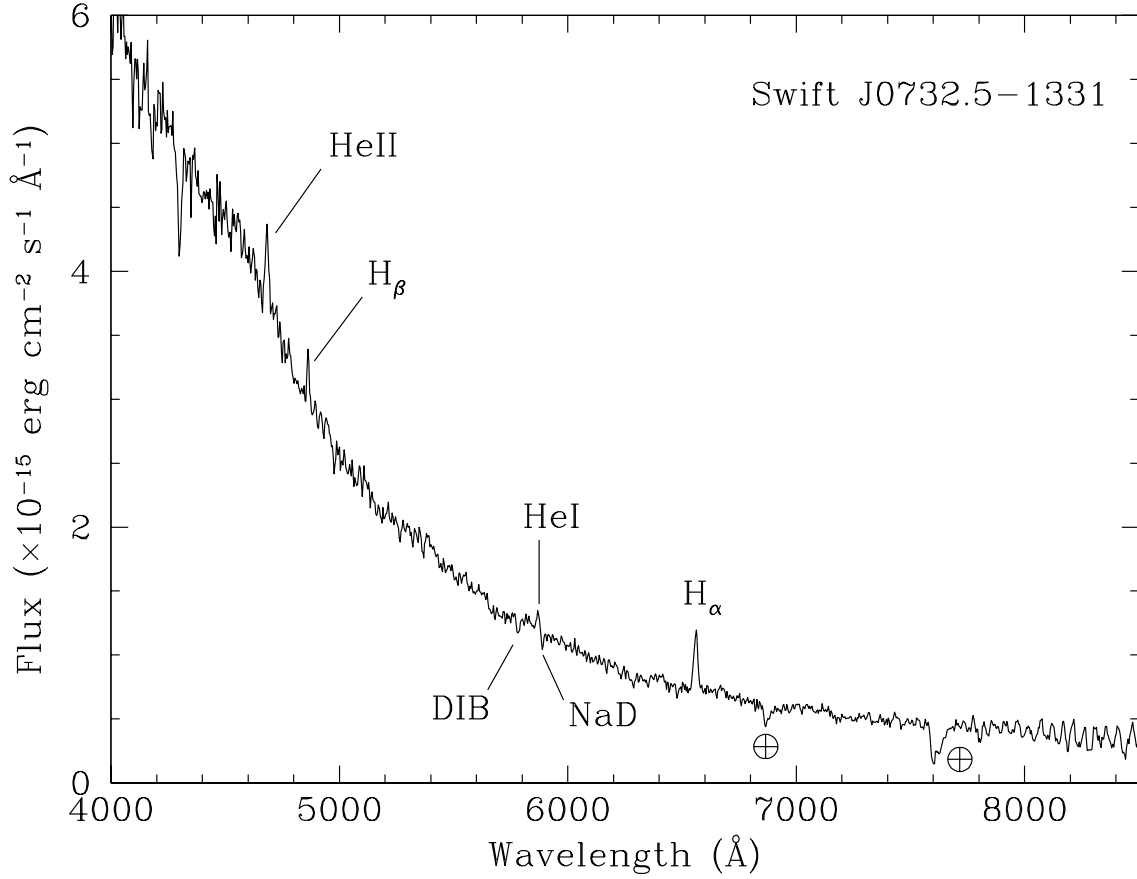


Fig. 16.— Spectrum (not corrected for the intervening Galactic absorption) of the optical counterpart of Swift J0732.9-1331. In the spectrum the main spectral features are labeled. The symbol  $\oplus$  indicates atmospheric and telluric features.